

Using OpenStreetMap (OSM) to Enhance the Classification of Local Climate Zones in the Framework of WUDAPT

Cidália Fonte^{1,2}, Patrícia Lopes¹, Linda See³ and Benjamin Bechtel⁴

1 Department of Mathematics, University of Coimbra, P-3001-501 Coimbra, Portugal

2 INESC Coimbra, P-3030-290 Coimbra, Portugal

3 Ecosystems Services and Management Program, International Institute for Applied Systems Analysis, Schlossplatz 1, A-2361 Laxenburg, Austria

4 Department of Geography, Ruhr-University Bochum, 44801 Bochum, Germany

Abstract

The World Urban Database and Access Portal Tools (WUDAPT) project has adopted the Local Climate Zone (LCZ) scheme as a basic and consistent description of form and function of cities at neighbourhood scale. LCZs are classified using crowdsourced training samples, open data and open source software but the quality of the maps still needs improvement. The aim of this paper is to investigate the use of data from OpenStreetMap (OSM) to enhance the development of LCZs, complement the existing data sources, and improve the accuracy of the maps. Various features were derived from the OSM database and combined with seasonal LCZ maps. Therefore a methodology was developed and tested for Hamburg, Germany, using a fuzzy approach and then a weighted combination method was applied to combine the inputs from OSM with each of the seasonal LCZ maps. The results showed that improvements can be achieved for certain classes, either in terms of accuracy, e.g. rectifying the misclassification of agricultural areas as heavy industry, or representation on the map, e.g. a more detailed water network. The approach developed is flexible and allows for knowledge about which data sources are more reliable as inputs to the combination and weighting process.

Keywords: Local Climate Zones, Remote Sensing, World Urban Database and Access Portal Tools (WUDAPT), Volunteered Geographic Information, OpenStreetMap

1. Introduction

Cities are particularly vulnerable to increasing temperatures from climate change because of a phenomenon known as the Urban Heat Island (UHI) effect (Oke, 1967), which is the result of higher amounts of impervious surfaces, a lack of vegetation in urban areas and the presence of concentrated urban structures. UHIs occur in almost all urban areas, large or small, and in warm or cold climates (Stewart and Oke, 2012). A cause for concern is that UHIs can affect human health and well-being, and heat waves in urban areas have contributed to loss of life. For example, during the heat wave in 2003, more than 30,000 people in Europe died (UNEP, 2004). These events will be even more pronounced in the future as population continues to increase to 9.8 billion by 2050 and 11.2 billion by 2100 (UN Department of Economic and Social Affairs, 2017). Climate change will further exacerbate the heat risk. Future climate scenarios from the Intergovernmental Panel on Climate Change (IPCC)

indicate higher frequency and duration of heat waves in the coming decades, which will continue to increase health risks (Revi et al., 2014). Other negative effects include increases in air pollution and the general reduction in thermal comfort (Harlan and Ruddell, 2011).

The UHI effect has been extensively studied in the literature; see e.g. the comprehensive literature review of more than 100 UHI studies in the USA, Asia, Africa, Australia and Europe, all of which show higher temperatures in urban versus rural areas (Tzavali et al., 2015). Different types of UHI need to be distinguished. The most commonly studied type is the canopy layer UHI, which is studied using air temperature records from weather stations or mobile sensors (see Santamouris (2014) for a comparison of about 75 studies). The second type is the surface UHI, which is investigated by the use of thermal infrared remote sensing (Ngie et al., 2014; Tomlinson et al., 2011), which provides comprehensive spatial coverage but also trade-offs between spatial and temporal coverage (Bechtel et al., 2012).

The UHI effect is estimated by comparing urban and rural values or their background temperatures, which is the difference between the maximum urban temperature and the surrounding rural temperatures (Oke, 1982; Oke et al., 2017). Thus for decades, typical UHI measurement studies have been based on the comparison of "urban" and "rural" air temperatures. However, the terms urban and rural cannot be defined universally since they do not have a unique objective meaning, and hence no climatological relevance. Furthermore, what is defined as urban or rural in one city can be different when applied to another city (Stewart and Oke, 2012). Hence the relation between urban and rural should be more precisely represented as a continuum as opposed to a dichotomy (Gugler, 1996). Thus, to provide a universal system applicable to urban temperature studies, Stewart and Oke (2012) established the Local Climate Zone (LCZ) classification system, which is based on a number of factors that capture the physical characteristics of the region. LCZs are also associated with a range of values for a number of different urban parameters, which have been used in different urban climate models, e.g., the Weather and Research Forecasting (WRF) meso-scale model (Brousse et al., 2016; Hammerberg et al., 2018), COSMO-CLM (Wouters et al., 2016) and SUEWS (Alexander et al., 2016), all of which can be used to study the UHI phenomenon.

The World Urban Database and Access Portal Tools (WUDAPT) project was initiated in 2009 with a particular emphasis on providing data on urban areas globally, where urban climate modelling is one application. The aim of WUDAPT is to collect data on the form and function of cities around the world. It has adopted the LCZ classification scheme because it is culturally neutral, provides a standardized way of comparing cities around the world and can be generated using open source tools and open data. Moreover, WUDAPT encourages local experts around the world to participate in populating the WUDAPT database with information about their own cities (Ching et al., 2018).

The WUDAPT methodology uses Landsat 8 satellite images, and a workflow based on Google Earth and SAGA GIS software, which is described in more detail in Bechtel et al. (2015) and on the WUDAPT web page (<http://www.wudapt.org>). The method involves creating training sites for each LCZ class present in the region of interest and then classifying the Landsat images using a random forest classifier. Much recent attention has been paid to finding ways to quality assure the resulting LCZ maps (Bechtel et al., 2017, 2019), which indicates that there is still room for improvement.

Recently there have been various developments in trying to improve the methodology for the generation of LCZ maps, which in particular comprise new methods, upscaling and

transfer-learning, and new input data. The methodological development has focused on new and more sophisticated classifiers and post-processing techniques including context classifiers (Verdonck et al., 2017), residual convolutional neural networks (Qiu et al., 2018), and Markov random fields (Tuia et al., 2017b). Moreover, alternative approaches from supervised classification have been tested, in particular GIS-based methods (Gal et al., 2015; Geletič and Lehnert, 2016; Hidalgo et al., accepted; Lelovics et al., 2014; Unger et al., 2014; Zheng et al., 2018). A particular focus was set on transferring training labels between cities (Demuzere et al., 2019; Kaloustian et al., 2017; Xu et al., 2017) and developing robust and transferable classifiers, which was also the challenge of the 2017 Data Fusion Contest (Tuia et al., 2017a; Yokoya et al., 2018), organized by the Image Analysis and Data Fusion Technical Committee of the IEEE Geoscience and Remote Sensing Society. Further work has been done on the upscaling and generation of large area data sets (Demuzere et al., in review; Qiu et al., 2018). On the data side different sensors have been tested in the classic approach, including Sentinel 2 (Demuzere et al., 2019; Kaloustian et al., 2017; Qiu et al., 2018), ASTER (Yong Xu et al., 2017), SAR (Bechtel et al., 2016; Demuzere et al., 2019; Kaloustian et al., 2017) and nighttime lights (Demuzere et al., 2019; Qiu et al., 2018), and various remote sensing derived parameters were used in Mitraka et al. (2015).

One particular open data source that may benefit the generation of LCZ maps is OpenStreetMap (OSM), which was also used by some teams in the Data Fusion Contest (Sukhanov et al., 2017; Yokoya et al., 2018) and is an example of volunteered geographic information (VGI) (Goodchild, 2007) in which millions of citizens have contributed to creating an online vector map of the world (Jokar Arsanjani et al., 2015). OSM began in 2004, where the fundamental goal is to build an open and free database of geographic information (Coast, 2005; Haklay and Weber, 2008; Jokar Arsanjani et al., 2015). OSM volunteers contribute and maintain data on roads, railways, buildings, land use and many other types of information around the world. OSM data are available under an Open Database (ODbL) license, which allows for commercial use of the data as long as a reference is made to the OSM project and the data, and any derivative products are released under the same license or another compatible one (<https://www.openstreetmap.org/>). OSM has been used in a number of different applications including generation of land cover and land use maps (Fonte et al., 2017a; Schultz et al., 2017; Grippa et al., 2018), in a large number of quality assessment studies (Girres and Touya, 2010; Haklay et al., 2010; Fan et al., 2014; Mooney, 2015) and even in the generation of LCZs (Lopes et al., 2017; Samsonov and Trigub, 2017). Hence the aim of this paper is to investigate how OSM can be used to enhance the LCZ classification process and improve the accuracy of the resulting maps. Since OSM is freely available, the use of this data source also aligns well with the goals of the WUDAPT project.

2. The Local Climate Zone (LCZ) system

The LCZ classification system divides the landscape into seventeen classes (see Table 1), which are defined as areas of “uniform surface cover, structure, material, and human activity that span from hundreds of meters to several kilometers in horizontal scale” (Stewart and Oke 2012, p.1884). Ten classes are built-up types (from LCZs 1 to 10) while the remaining seven are land cover types (LCZs A to G), and there is an additional variable to denote seasonal properties, e.g. LCZ 1s would refer to LCZ 1 when the surface is covered by snow.

All classes emerge from the logical division of the landscape according to different properties that influence the screen-height temperature, i.e. the temperature measured one to two meters

above the ground (Stewart et al., 2014), such as surface structure and surface cover. LCZ types can be distinguished by ranges of typical values of measurable physical properties, which characterize the geometry and surface cover, and the thermal, radiative and anthropogenic energy features of the surface.

Table 1- Local Climate Zone classes and definitions as proposed by Stewart and Oke (2012).

LCZ classes	Definition	
Built types	Compact high-rise (LCZ 1)	Dense mix of tall buildings to tens of stories. Few or no trees. Land cover mostly paved. Concrete, steel, stone, and glass construction materials.
	Compact midrise (LCZ 2)	Dense mix of midrise buildings (3–9 stories). Few or no trees. Land cover mostly paved. Stone, brick, tile, and concrete construction materials.
	Compact low-rise (LCZ 3)	Dense mix of low-rise buildings (1–3 stories). Few or no trees. Land cover mostly paved. Stone, brick, tile, and concrete construction materials.
	Open high-rise (LCZ 4)	Open arrangement of tall buildings to tens of stories. Abundance of pervious land cover (low plants, scattered trees). Concrete, steel, stone, and glass construction materials.
	Open midrise (LCZ 5)	Open arrangement of midrise buildings (3–9 stories). Abundance of pervious land cover (low plants, scattered trees). Concrete, steel, stone, and glass construction materials.
	Open low-rise (LCZ 6)	Open arrangement of low-rise buildings (1–3 stories). Abundance of pervious land cover (low plants, scattered trees). Wood, brick, stone, tile, and concrete construction materials.
	Lightweight low-rise (LCZ 7)	Dense mix of single-story buildings. Few or no trees. Land cover mostly hard-packed. Lightweight construction materials (e.g., wood, thatch, corrugated metal).
	Large low-rise (LCZ 8)	Open arrangement of large low-rise buildings (1–3 stories). Few or no trees. Land cover mostly paved. Steel, concrete, metal, and stone construction materials.
	Sparsely built (LCZ 9)	Sparse arrangement of small or medium-sized buildings in a natural setting. Abundance of pervious land cover (low plants, scattered trees).
	Heavy industry (LCZ 10)	Low-rise and midrise industrial structures (towers, tanks, stacks). Few or no trees. Land cover mostly paved or hard-packed. Metal, steel, and concrete construction materials.
Land cover types	Dense trees (LCZ A)	Heavily wooded landscape of deciduous and/or evergreen trees. Land cover mostly pervious (low plants). Zone function is natural forest, tree cultivation, or urban park.
	Scattered trees (LCZ B)	Lightly wooded landscape of deciduous and/or evergreen trees. Land cover mostly pervious (low plants). Zone function is natural forest, tree cultivation, or urban park.
	Bush, scrub (LCZ C)	Open arrangement of bushes, shrubs, and short, woody trees. Land cover mostly pervious (bare soil or sand). Zone function is natural scrubland or agriculture.
	Low plants (LCZ D)	Featureless landscape of grass or herbaceous plants/crops. Few or no trees. Zone function is natural grassland, agriculture, or urban park.
	Bare rock or paved (LCZ E)	Featureless landscape of rock or paved cover. Few or no trees or plants. Zone function is natural desert (rock) or urban transportation.
	Bare soil or sand (LCZ F)	Featureless landscape of soil or sand cover. Few or no trees or plants. Zone function is natural desert or agriculture.
	Water (LCZ G)	Large, open water bodies such as seas and lakes, or small bodies such as rivers, reservoirs, and lagoons.
Variable land cover properties	Bare trees (b)	Leafless deciduous trees (e.g., winter). Increased sky view factor. Reduced albedo.
	Snow cover (s)	Snow cover >10 cm in depth. Low admittance. High albedo.
	Dry ground (d)	Parched soil. Low admittance. Large Bowen ratio. Increased albedo.
	Wet ground (w)	Waterlogged soil. High admittance. Small Bowen ratio. Reduced albedo.

3. Data and methodology

The methodology developed here consists of the following four steps: 1) Creation of four LCZ maps for the study area using the methodology proposed by the WUDAPT project, using four images corresponding to different astronomical seasons (winter, spring, summer and autumn); 2) conversion of OSM features into LCZ classes; 3) integration of the data obtained from the previous two steps; and 4) an accuracy assessment. These steps are described in more detail below.

3.1 Study area and data

The study area used to test the methodology proposed in this paper is a section from the city of Hamburg in Germany. Hamburg is located in the North German Plain on the lower slopes of the Elbe River, 80 km upstream of the Elbe estuary. It is the second largest city in Germany after Berlin, with 755.3 km² and a population of 1,814,597 inhabitants (Rose and Wilke, 2015; Statistical Office of Hamburg and Schleswig-Holstein, 2014). Figure 1 **Erro! A origem da referência não foi encontrada.** shows the four Landsat 8 satellite images of the area that were used to create the LCZ maps as outlined in sections 3.2 to 3.4. These images were downloaded from the USGS Earth Explorer website.

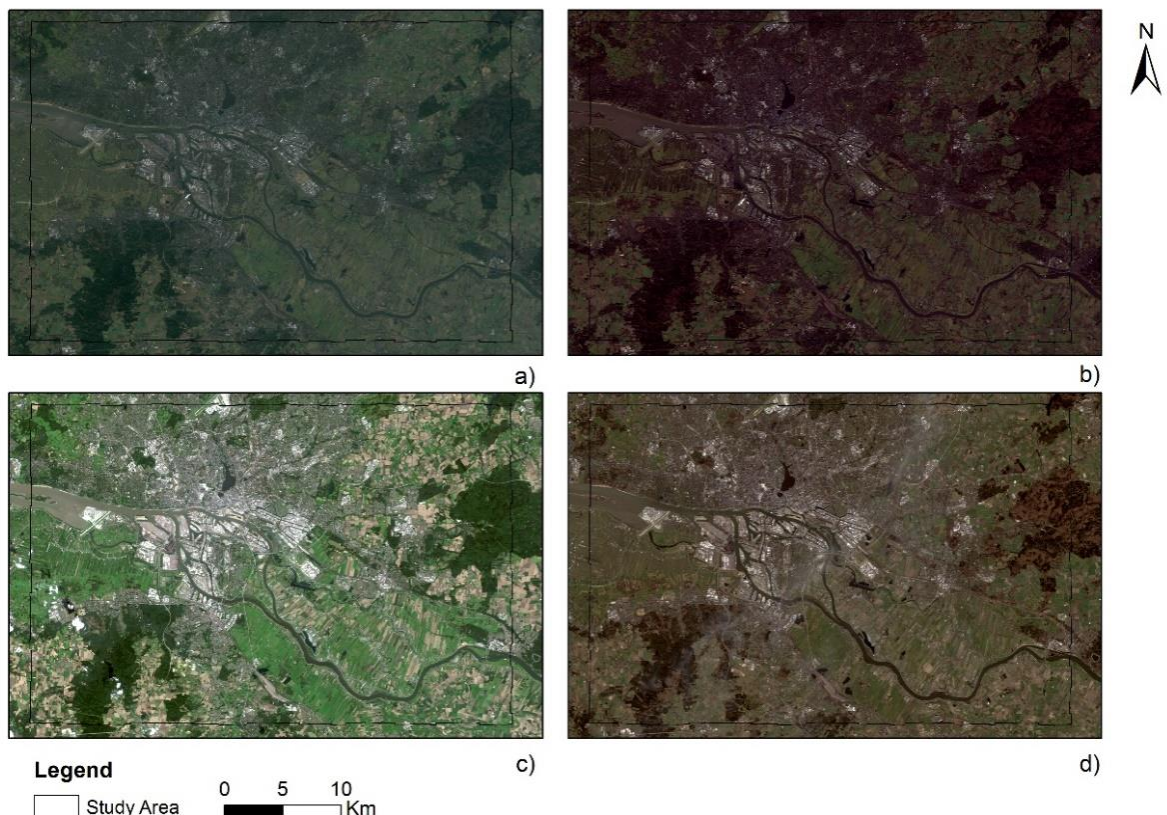


Figure 1 - Landsat 8 true color imagery of Hamburg in a) winter - 2017, January 3rd, b) autumn - 2014, December 6th, c) summer - 2015, August 21st and d) spring - 2016, April 30th.

This area was chosen because it has good coverage of OSM data (see Figure 2 **Erro! A origem da referência não foi encontrada.**). The information available in OSM is in vector format and each element has an associated spatial dimension (i.e. geometry) and attribute data. When an OSM contributor creates an object that represents a real-world feature, the

volunteer is able to use three types of primitives: nodes (points), ways (polylines, closed ways or areas/polygons) and relations (logical collections of two or more nodes, ways, areas or other relations) (Neis and Zielstra, 2014). Each of these primitives are associated with one or more attributes, also referred to as tags. Tags are used to describe information such as the type of object (e.g. restaurant, street, etc.) and their most relevant details (e.g. address, if access is restricted, etc.). Each tag is formed by a key and a value; e.g. to identify a wood, the tag "natural=wood" may be used, where "natural" is the key and "wood" is the value. OSM contributors can use their own tags, although there is a suggested list of tags that have been established and agreed by the OSM community, which includes explanations and examples of their use (OpenStreetMap Wiki contributors, 2018).

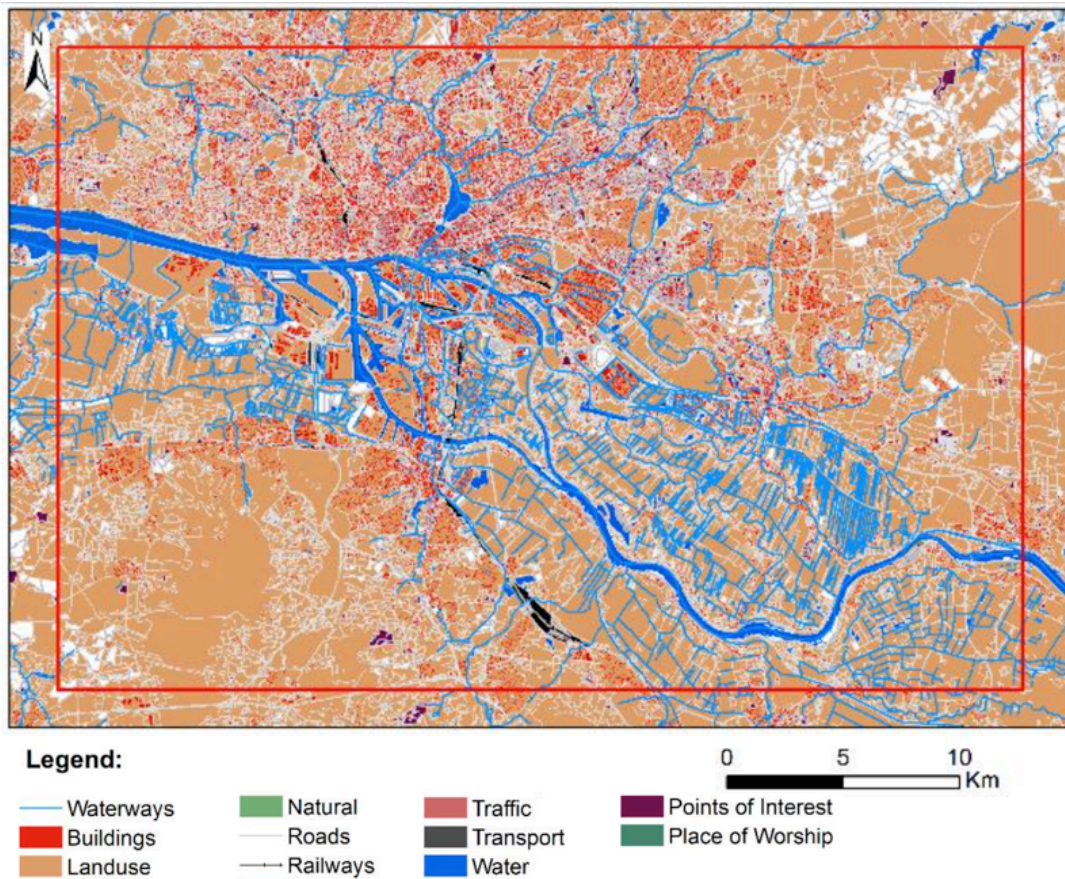


Figure 2 – Data available from OpenStreetMap (OSM) for the study area of Hamburg, Germany. Copyright: OSM contributors.

3.2 Creation of LCZ maps using WUDAPT

The first step in the methodology consists of generating the LCZ maps using the approach suggested by the WUDAPT project (Bechtel et al., 2015). Unlike the standard WUDAPT approach, no multi-seasonal input data were used to generate an all-year static LCZ map. Instead, separate LCZ maps were created using images from four different dates, corresponding to autumn, winter, spring and summer as shown in Figure 1. This was done for two reasons. First, this study aims to develop a fuzzy scheme in order to test the added value of OSM data, which means several input data sets of varying quality are needed to introduce some noise into the procedure. Secondly, this allows the influence of seasonally differing land cover to be studied, which is a known problem related to WUDAPT level 0 data (Bechtel et al.,

2019) and causes problems in some applications such as surface urban heat island modelling (Bechtel et al., in review). A cell size of 120m was used for the classification, as suggested by guidance provided by the WUDAPT project in 2016 although a cell size of 100m is now being routinely used. The application of a post classification 200m to 300m majority filter is also recommended. Therefore, as the cell size used here was 120m, a majority filter of 5x5 cells (corresponding to 25 neighbouring cells) was applied.

3.3 Conversion of OSM data into LCZs

The conversion of the OSM data into LCZ classes, or data that can assist in the LCZ classification process, is performed in two phases: namely data pre-processing and data processing. Some of this procedure has been documented previously in Lopes et al. (2017) while other parts of the methodology are introduced here.

3.3.1 Data pre-processing phase

The data pre-processing phase includes: the download of OSM data, identification of the key/value combinations that can be used to identify LCZ classes, the transformation of reference systems, and the creation of a vector grid corresponding to the pixels obtained from the application of the WUDAPT methodology. The latter operation is undertaken so that the outputs of the conversion of OSM data into the LCZ classes can be compared with the results from the satellite image classification.

To associate the OSM data with the LCZ classes, the key/value combinations and their descriptions, which were established by the OSM community (OpenStreetMap Wiki contributors, 2018), must be associated with the most relevant LCZ classes as part of a pre-processing step. It should be noted that, in some cases, the data available in OSM do not allow for a differentiation between LCZ classes. For example, the OSM features that correspond to regions with trees do not allow for differentiation between dense or scattered trees, and therefore it is not possible to choose between class A (dense trees) or B (scattered trees). Therefore, in cases such as this, the conversion process simply identifies the most likely classes to which these regions in OSM may be associated.

As volunteers can create new values for the available keys on a continuous basis, the initial association of key/value combinations with LCZ classes may be insufficient, as new pairs of keys/values may exist for the region of interest. Moreover, even for the same region, since OSM is constantly being edited by volunteers, data may differ if obtained at different dates. Thus, this pre-processing step must be repeated over time.

The OSM data were downloaded from the Geofabrik portal (<http://www.geofabrik.de>) in shapefile format. Table 2 shows the associations considered for the study area, corresponding to the tags found in the data downloaded.

The next step in the pre-processing phase is to re-project the LCZ maps to the same reference system as OSM so that they can be compared and integrated. A vector grid (referred to from now on as GRID) is then created in such a way that each vector cell corresponds to a pixel in the LCZ map.

Table 2. Correspondence between LCZ classes and OSM keys and values.

LCZ class	OSM key	Key values
LCZ A or B	Natural	Wood, trees, grass, tree_row, forest
	landuse	Forest, nature_reserve
LCZ C	natural	Scrub
	landuse	Heath, orchard, scrubs, vineyard, scrub, scrubs, plant_nursery
LCZ D	natural	Grass
	landuse	Farm, farmland, farmyard, meadow, greenfield, grass
LCZ G	natural	Water
	landuse	river, stream, canal, drain, brook, ditch, riverbank
LCZ 1 to 10	roads	Bus_guideway, living_street, primary, primary_link, residential, raceway, road, secondary_link, tertiary, tertiary_link, trunk, trunk_link
	railways	funicular, miniature, monorail, light_rail, narrow_gauge, rail, tram, transfer_table, mainline
	building	apartments, hotel, house, detached, residential, dormitory, terrace, houseboat, static_caravan, commercial, industrial, retail, warehouse, bakehouse, cathedral, chapel, church, mosque, temple, synagogue, shrine, civic, hospital, school, stadium, train_station, transportation, university, barn, public, bridge, bunker, cabin, ruins, construction, farm_auxiliary, garage, garages, carport, hangar, roof, shed, stable, transformer_tower, kiosk

3.3.2 Data processing phase

In the processing phase, the conversion of the OSM data into the LCZ classes is undertaken. This phase consists of several steps, as different features available in OSM require different processing approaches. Some OSM features have a direct association to LCZ classes, namely to the land cover classes such as LCZ A or B (dense trees and scattered trees), LCZ C (Bush or scrub) or LCZ D (low plants). The processing of these features requires the selection of the OSM polygons with a particular combination of key/value that satisfies the defined correspondences to the LCZ classes. Once all polygons corresponding to the LCZ classes are identified, they are merged into a single feature. Then an intersection of the resulting features with the GRID corresponding to the satellite image classification is undertaken, and the area occupied by the specified LCZ in each cell of the GRID is computed. Figure 3, shows the procedure used to derive LCZ A or B. Schemas of the methodology used to identify LCZ C and LCZ D are provided as supplementary materials to the article.

Some of the features in OSM are represented by linear elements, such as roads, railways and waterways. To assign these features to classes in an LCZ map, they need to be converted into areas. This process was done by clipping these features within the study area and creating a buffer around them. To define the width of the buffers to use so that the resulting areas do not overlap other types of features in the surrounding areas, in particular the buildings along the streets, the lines are separated into segments (using available GIS tools, such as “Explode lines” in QGIS or “Split Line At Vertices” in ArcGIS), the distance of each segment to the OSM buildings is computed, and the result is assigned to each segment as an additional attribute (distance to buildings) (Fonte et al., 2017b). The process used to create the buffers is illustrated in Figure 4, where “d” represents the distance to the buildings and “t” represents a predefined value for each type of feature, which is used when distance “d” is too large to be considered. If the distance (d) of the feature to the buildings is greater than the user-defined threshold (t), then there are no buildings near the feature, and the value “t” is used to create

the buffer. If the distance to buildings (d) is below this threshold, then “ d ” is used to define the buffer. The threshold values need to be chosen according to the characteristics of the regions under analysis, as different types of features may have very different typical widths in different cities and different parts of the world.

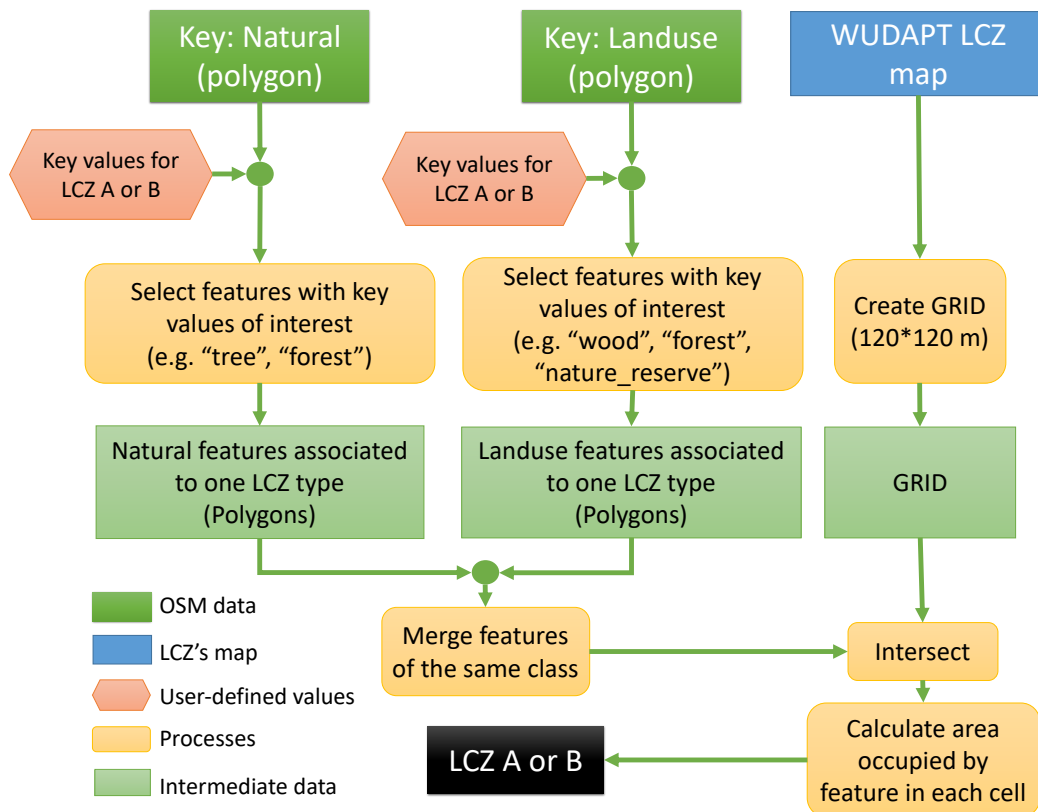


Figure 3 - Schematic of the methodology used for the conversion of OSM data into LCZ classes A (Dense trees) or B (Scattered trees).

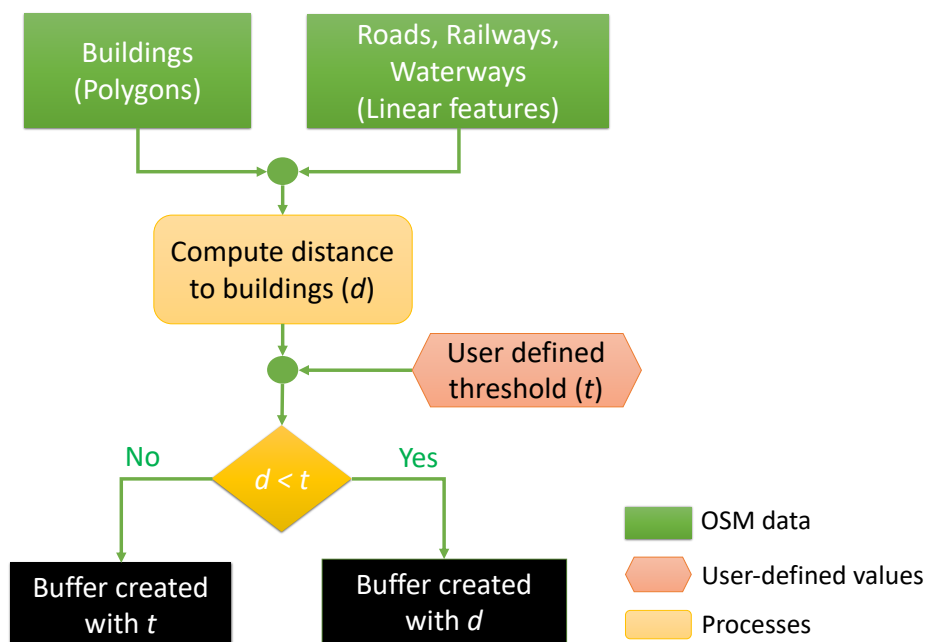


Figure 4 - Procedure for converting linear features into polygons

For LCZ G (Water), there are usually both linear features representing waterways and polygonal features corresponding to the regions with water (mainly in the features with the key “natural”) in OSM. Hence, it is necessary to convert these linear features to areas, and then merge them into polygonal features that also represent water. A schema illustrating the procedure used to extract the water layer from the OSM data is available as supplementary material to this article. As with the other classes, the merged results are then combined with the outputs obtained with the GRID previously created at a spatial resolution of 120 m. An intersection of the GRID with the data obtained is then made, and the percentage of the cell area occupied by each feature was computed for all cells.

For the LCZ urban classes (LCZ 1 to LCZ 10), the data available in OSM can provide information on the presence of buildings and impervious surfaces, such as roads or railways. To associate these data with the LCZ classes, the values established by Stewart and Oke (2012) regarding the building surface fraction and the impervious surface were considered. Figure 5 illustrates the procedure used to extract the urban classes from the OSM data.

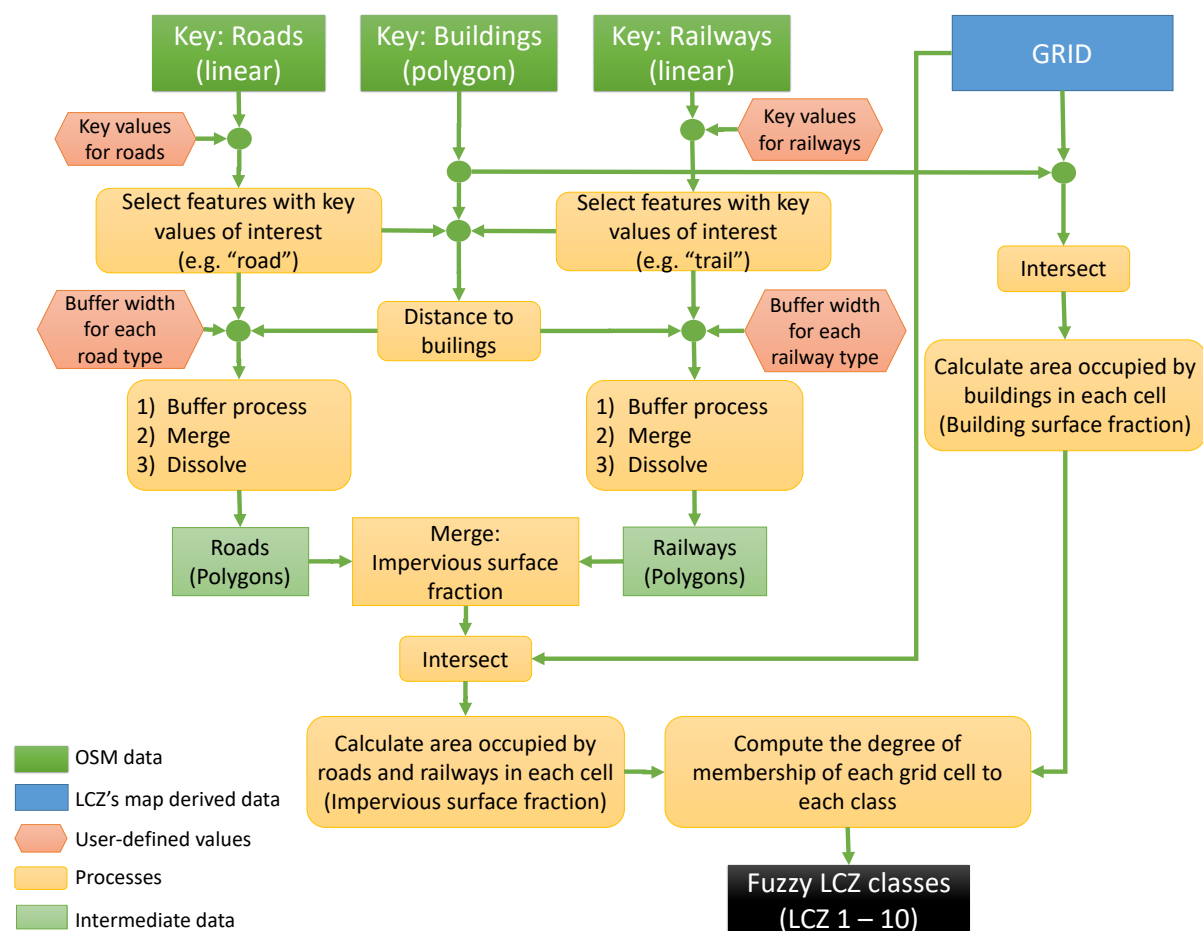


Figure 5 - Schematic of the methodology used to convert OSM data into fuzzy classes LCZ 1 to 10

The data resulting from the conversion of the road and railway features to areas was aggregated, which correspond to impervious regions. The buildings existing in OSM were extracted and the layer corresponding to the impervious regions and the buildings were

intersected with the GRID corresponding to the cells in the raster file resulting from the classification of the satellite images. The percentage of each cell occupied by the impervious layer and building was then computed, generating two layers: the Building Surface Fraction (BSF) and the Impervious Surface Fraction (ISF).

Once the information about the BSF and ISF in each cell of the GRID is available, a degree of membership of each cell in each of the LCZ urban classes was computed, considering the data in Table 3, which shows the BSF and ISF corresponding to each LCZ class, as defined by Stewart and Oke (2012).

Table 3 - Percentage of Building Surface Fraction (BSF) and Impervious Surface Fraction (ISF) for classes LCZ 1 to 10 (in Stewart and Oke 2012).

LCZ class	BSF (%)	ISF (%)
LCZ 1	40–60	40–60
LCZ 2	40–70	30–50
LCZ 3	40–70	20–50
LCZ 4	20–40	30–40
LCZ 5	20–40	30–50
LCZ 6	20–40	20–50
LCZ 7	60–90	< 20
LCZ 8	30–50	40–50
LCZ 9	10–20	> 20
LCZ 10	20–30	20–40

The degrees of membership of the BSF and ISF in each LCZ class were computed considering trapezoidal membership functions (Klir and Yuan, 1995). This approach was used because there is uncertainty associated with the correctness of the area occupied by the buildings and impervious areas in each cell in OSM. There may be buildings or roads missing in OSM or polygons present in the buildings layer by mistake. Therefore, the fact that the BSF and ISF do not correspond to the intervals indicated in Table 3 does not mean that the class is not present at that location. This is simply considered as one piece of evidence that has an associated uncertainty. Figure 6 shows the membership functions of the BSF and ISF for class LCZ 2 according to the data presented in Table 3.

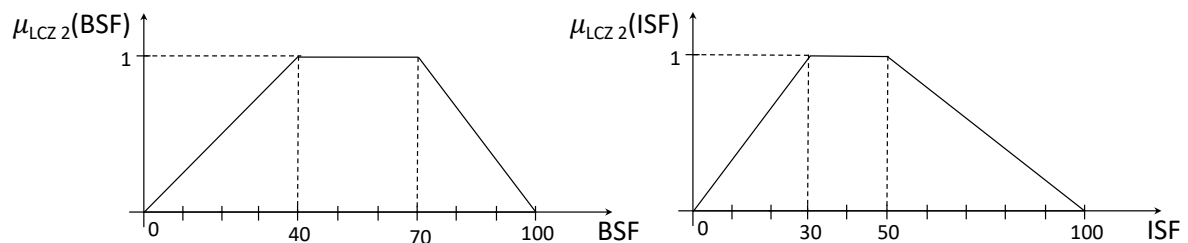


Figure 6 – Degree of membership to LCZ2 of the Building Surface Fraction (BSF) and Impervious Surface Fraction (ISF) based on the data in Table 3.

The degree of membership of a cell x to an urban LCZ class will then be obtained with the fuzzy standard intersection operator (fuzzy “and” operator) of the memberships of the BSF and ISF values obtained for that cell from OSM data, as both conditions need to be met simultaneously. For example, the degree of membership of cell x to LCZ 2 ($\mu_{LCZ 2}(x)$) will be

computed using equation (1), where $BSF(x)$ and $ISF(x)$ are, respectively, the BSF and ISF obtained for cell x using the OSM data.

$$\mu_{LCZ\ 2}(x) = \min[\mu_{LCZ\ 2}(BSF(x)), \mu_{LCZ\ 2}(ISF(x))] \quad (1)$$

According to equation (1), a cell with $BSF(x) = 30\%$ and $ISF(x) = 40\%$ would have, according to Figure 6, $\mu_{LCZ\ 2}(BSF(x)) = 0.75$ and $\mu_{LCZ\ 2}(ISF(x)) = 1$, therefore $\mu_{LCZ\ 2}(x) = \min(0.75, 1) = 0.75$. The degrees of membership to all LCZ built classes were computed using the same approach.

Degrees of membership to the land cover classes (LCZ classes A to G) are obtained considering the percentage of cell covered by the class for each LCZ class, as obtained using the procedures illustrated in Figure 3 and the corresponding approaches described for the other LCZ classes (available as supplementary materials), considering a linear membership function (Figure 7).

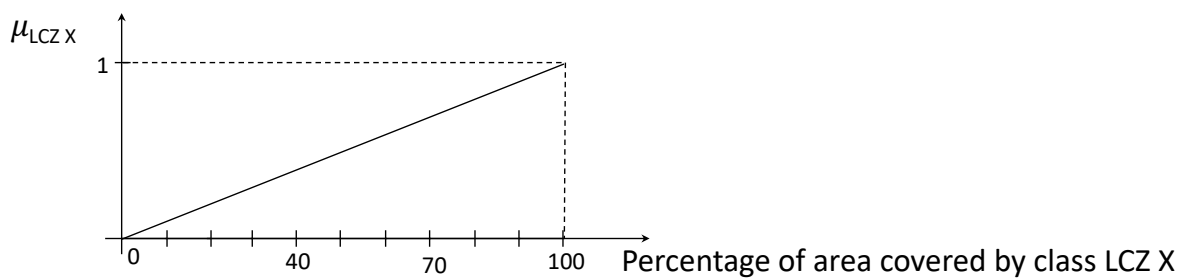


Figure 7 - Degree of membership to LCZ X (where X may be A, B, C, D, E, F or G) obtained as a function of the percentage of area covered by the class obtained from OSM data.

3.4 Integration and Combination of Data

3.4.1 Integration of the LCZ maps and the OSM data converted to LCZs

As outlined previously, four seasonal Landsat 8 images were classified using the WUDAPT methodology. As some physical characteristics of the territory such as vegetation change with the seasons, and this translates into different spectral responses for the same area at different times of the year, the classification of the four images produces different results for some locations, resulting in inconsistent results. To handle this inconsistency, all the data are now combined at the pixel level. For this combination, point features corresponding to the centroid of each pixel were created (see Figure 8). The classes obtained for each pixel with the classification of the winter, summer, autumn and spring images were then extracted and added as additional attributes to the table associated with these points. These data were then spatially joined to the GRID used in the conversion of the OSM data into LCZ classes. This operation enabled the aggregation of all the data available for each point feature to the polygons of the GRID that contained them.

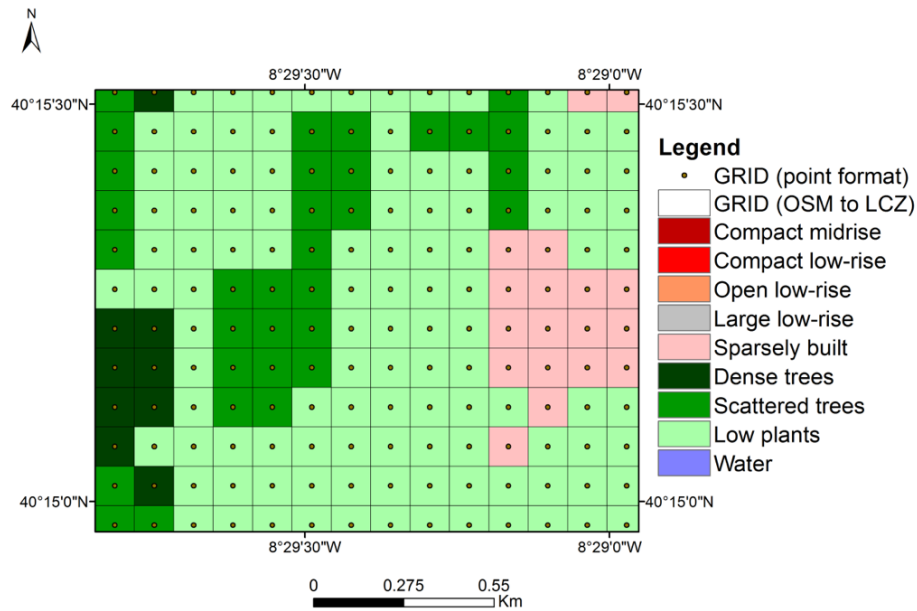


Figure 8 - Representation of the point features created and the vector GRID, overlaid with an LCZ map produced from the classification of one of the Landsat 8 images.

3.4.2 Combination of the previous results

To combine the evidence coming from all of the data associated with each point, a fuzzy logic approach is used, where $\mu_{LCZ X} Y(x)$ represents the reliability that, according to data source Y, pixel x belongs to LCZ class X. As some data sources may be more reliable than others for a particular class, different weights may be assigned to each data source for each class. Hence, the degree of reliability associated with the assignment of pixel x to class LCZ X is computed in equation (2), where $w_{Y X}$ is the weight associated with data source Y and class X and $\mu_{LCZ X} Y(x)$ is the degree of membership of pixel x in class X according to data source Y. As a hard classification was used in this case study, as recommended by the WUDAPT project, each pixel is assigned to only one class, and therefore the degrees of membership take on only values of one if the class is assigned to the pixel, or zero if not. However, a soft version of the classifier could be used, and the probabilities that are computed by the Random Forest classifier of assigning each pixel to the classes could be used instead. As outlined previously, four images were considered. Y is therefore expressed as *Win*, *Spr*, *Sum* and *Aut*, respectively, for the winter, spring, summer and autumn images, and *OSM* for the data extracted from OSM.

$$\begin{aligned}
 Rel_{LCZ X}(x) = & w_{Win X} \mu_{LCZ X} Win(x) + w_{Spr X} \mu_{LCZ X} Spr(x) \\
 & + w_{Sum X} \mu_{LCZ X} Sum(x) + w_{Aut X} \mu_{LCZ X} Aut(x) \\
 & + w_{OSM X} \mu_{LCZ X} OSM(x)
 \end{aligned} \quad (2)$$

The final class associated with each pixel can be obtained through equation (3), by choosing the class that scored the largest reliability value for that pixel:

$$FinalClass(x) = \max_{for\ all\ LCZ\ X} (Rel_{LCZ X}(x)) \quad (3)$$

This methodology for data integration requires choosing and then assigning weights to each data source for each class, which will be the parameters of the procedure. If the same degree of reliability is expected to come from all data sources for all classes, equal weights can be assigned to all, which is the default. However, if some data source is expected to have better

results for a particular class, such as a spring image for vegetation or OSM for water classes, then different weights can be associated with these data sources for these classes. If a particular data source has very unreliable data for a particular class, a weight of zero can also be considered, basically excluding that data source from the results for that class.

3.5 Accuracy Assessment

To assess the accuracy of all the maps, a reference database was created. A stratified sample was used, selecting 200 points per class, and the strata were the classes obtained with the classification of the winter images. The reference data were created through photo-interpretation of the images available in Google. Confusion matrices were created, computing estimations of the population true cell proportions \hat{p}_{ij} using the approach proposed by Card (1982) for stratified samples, shown in equation (4), where N_{i+} is the number of pixels in class i in the map, N is the total number of pixels in the map, n_{ij} is the number of pixels in the reference database assigned to class i in the map and class j in the reference database, and n_{i+} is the number of pixels in the sample assigned to class i in the map.

$$\hat{p}_{ij} = \left(\frac{N_{i+}}{N} \right) \left(\frac{n_{ij}}{n_{i+}} \right) \quad (4)$$

The user's accuracy (UA) and producer's accuracy (PA) per class as well as the overall accuracy (OA) were computed from the resulting confusion matrix using, respectively, formulas (5), (6) and (7), where c is the number of classes:

$$UA_i = \frac{\hat{p}_{ii}}{\sum_{j=1}^c \hat{p}_{ij}} \quad (5)$$

$$PA_j = \frac{\hat{p}_{jj}}{\sum_{i=1}^c \hat{p}_{ij}} \quad (6)$$

$$OA = \frac{\sum_{i=1}^c \hat{p}_{ii}}{\sum_{i=1}^c \sum_{j=1}^c \hat{p}_{ij}} \quad (7)$$

4. Results

4.1 Satellite image classification

Figure 9 shows the classification results of the winter, autumn, summer and spring images. Considerable differences can be identified, mainly for the urban classes LCZ 8 (large low-rise), LCZ 10 (heavy industry) and the land cover classes LCZ A (dense trees), LCZ B (scattered trees) and LCZ D (low plants). Figure 10 shows the regions that were assigned to the same class with the classification of all four images while Table 4 shows the area of these regions separated by class and by the total area of the region, the percentage of each of these regions relative to the total study area, as well as the percentage relative to the regions that were assigned to the class in at least one of the images. It can be seen that only 38.2% of the study area was classified in the same way when using the four images, and that these correspond to a percentage that varies between 3.0% and 44.1% of the regions that were assigned to the class at least once considering the four images, which shows the uncertainty in these results.

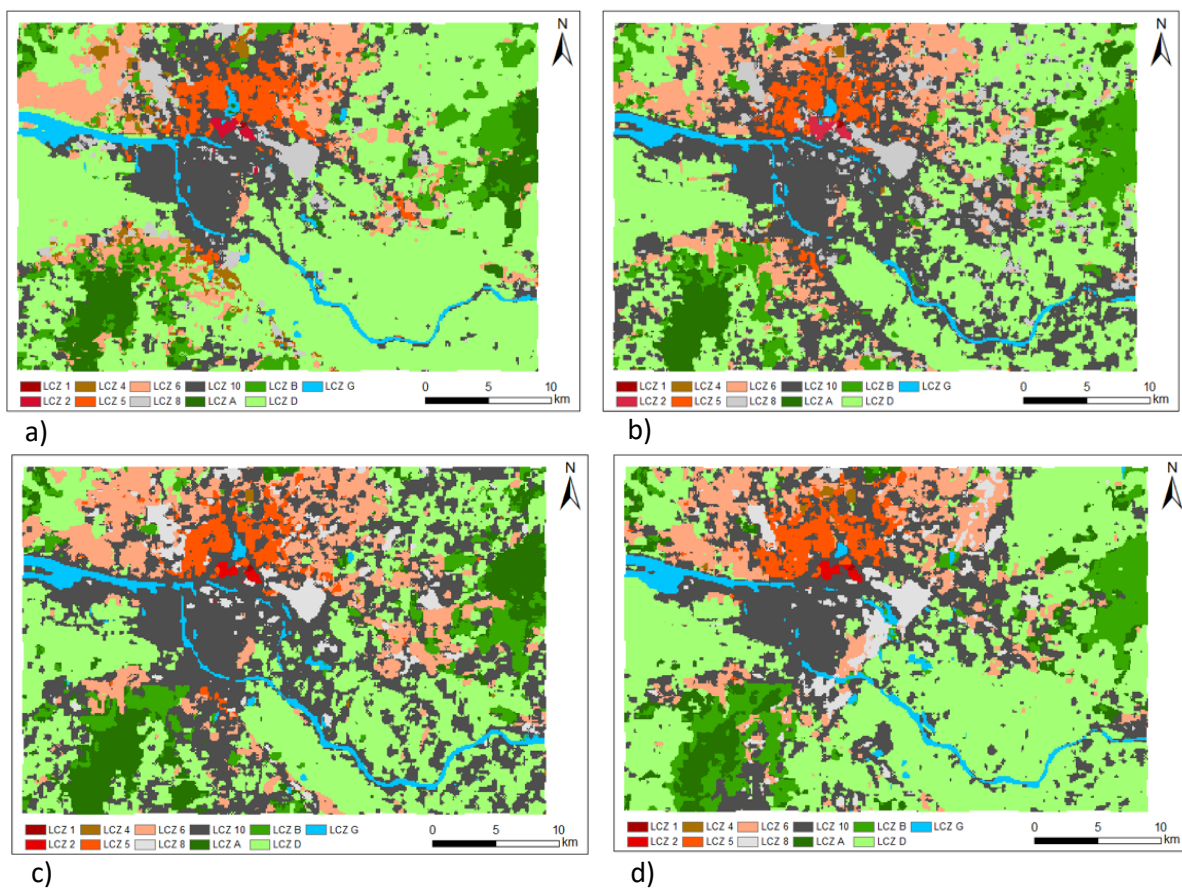


Figure 9 - LCZs maps for the city of Hamburg with a spatial resolution of 120 m, after applying a majority filter of twenty-five neighbouring cells for a) winter, b) autumn, c) summer and d) spring.

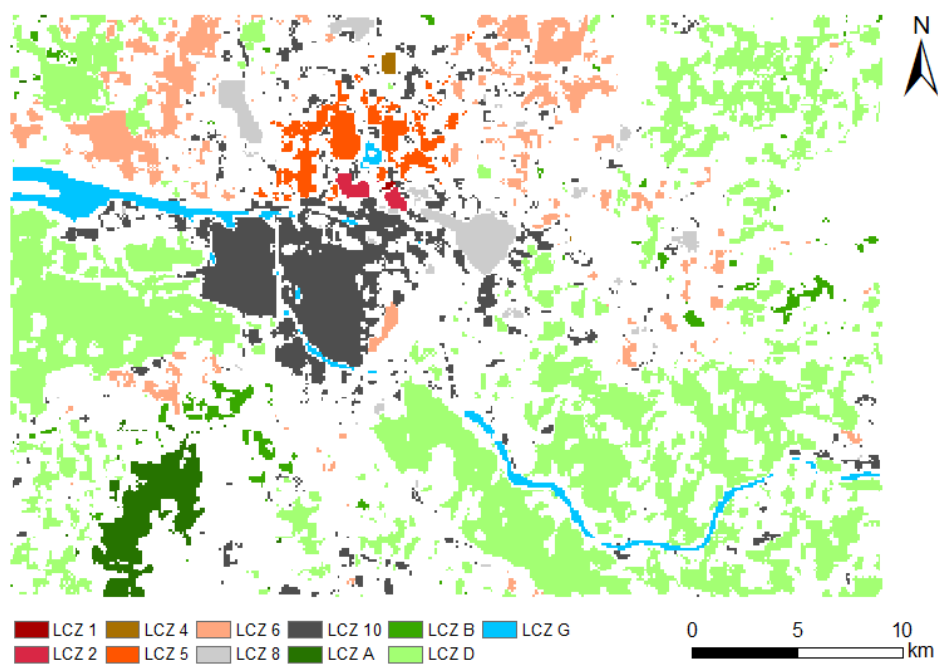


Figure 10 – Regions assigned to the same class with the classification of all images (winter, autumn, summer and spring).

Table 4 – Area (in km²), percentage (relative to the study area) of the regions assigned to the same class with the classification of all images, and the percentage of the region assigned to the same class in at least one image (union per class of the four classifications).

LCZ class	Area (km ²)	Percentage of the study area	Percentage of region assigned to the class by at least one image
LCZ 1 - Compact high-rise	0.2	0.0	33.9
LCZ 2 - Compact midrise	2.3	0.2	44.1
LCZ 4 - Open high-rise	0.8	0.1	3.0
LCZ 5 - Open midrise	16.9	1.3	23.3
LCZ 6 - Open low-rise	53.1	3.9	19.4
LCZ 8 - Large low-rise	17.3	1.3	13.0
LCZ 10 - Heavy industry	87.9	6.5	12.1
LCZ A - Dense trees	20.8	1.5	12.9
LCZ B - Scattered trees	11.5	0.9	6.3
LCZ D - Low plants	284.7	21.1	37.7
LCZ G – Water	19.4	1.4	39.2
Sum	514.9	38.2	-
Region with different classifications	833.1	61.8	-
Total	1348.0	100.0	-

The reference database (as explained in section 3.5) was used to assess the accuracy of the classified images. Table 5 shows the results, where it can be seen that the best results were obtained for the LCZ map created from the winter image, with an overall accuracy of 69%. The overall accuracy of the LCZ maps created from the other images was between 53% and 58%, with the worst result obtained for the autumn image. Some classes were classified particularly poorly, e.g. LCZ 4 (Open high-rise) in the autumn image (5% for user's accuracy and 8% for producer's accuracy) and in the spring image (6% for user's accuracy and 8% for producer's accuracy), as well as LCZ 2 (Compact midrise) with a producer's accuracy of 2% in the autumn image and 1% in the summer and spring images.

Table 5 – User's accuracy (UA), Producer's Accuracy (PA) and Overall accuracy of the LCZ classification of the winter, autumn, summer and spring images.

LCZ class	Winter image		Autumn image		Summer image		Spring image	
	UA	PA	UA	PA	UA	PA	UA	PA
LCZ 1	79	31	84	63	79	87	76	77
LCZ 2	78	8	74	2	62	1	65	1
LCZ 4	82	28	5	8	5	100	6	8
LCZ 5	77	67	51	19	51	9	53	18
LCZ 6	45	60	45	28	48	46	37	44
LCZ 8	80	41	63	72	56	86	55	70
LCZ 10	67	60	77	18	78	12	68	12
LCZ A	68	65	47	95	58	87	44	89
LCZ B	51	47	48	12	29	15	39	15
LCZ D	76	95	62	58	57	58	67	51
LCZ G	72	69	52	100	64	100	60	100
Overall accuracy	69		53		58		54	

4.2 Conversion of OSM data to LCZ classes

The conversion of the data extracted from OSM to LCZ classes was performed as described in section 3.3. Figure 11 shows the BSF and ISF obtained for the study area using the data extracted from OSM. Figure 12 shows the degrees of membership obtained for classes LCZ 4 (Open high-rise), LCZ 10 (Heavy industry), LCZ D (Low plants) and LCZ G (Water), which illustrate the results obtained for all classes. It can be seen that for these classes, most urban

areas have degrees of membership larger than zero for LCZ classes 4 and 10, as expected based on the methodology used. However, most regions in the centre of the city have higher degrees of membership to LCZ class 10 (Heavy industry). For LCZ D (Low plants) and LCZ G (Water), well-defined regions with high degrees of membership were obtained. In particular for LCZ G (Water), a very well-defined network of water bodies can be seen (Figure 12d).

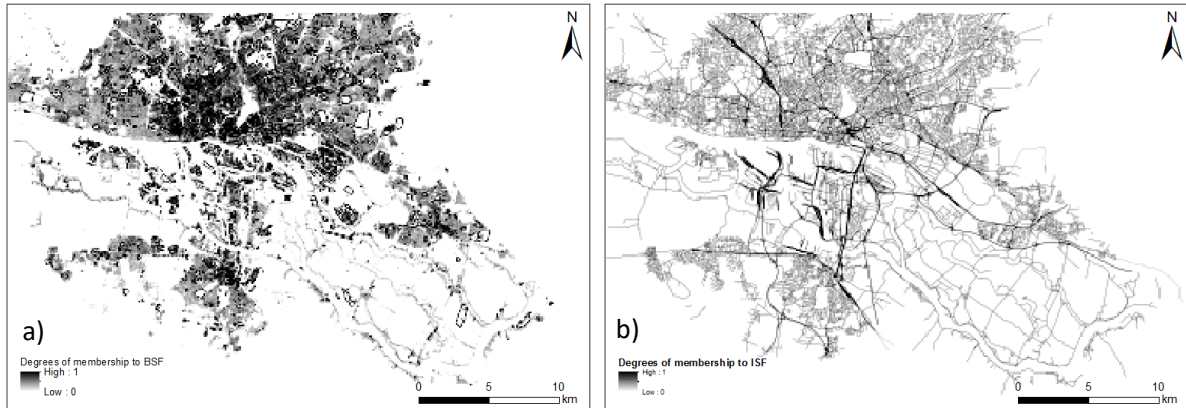


Figure 11 – a) Building Surface Fraction (BSF) and b) Impervious Surface Fraction (ISF) computed with OSM data.

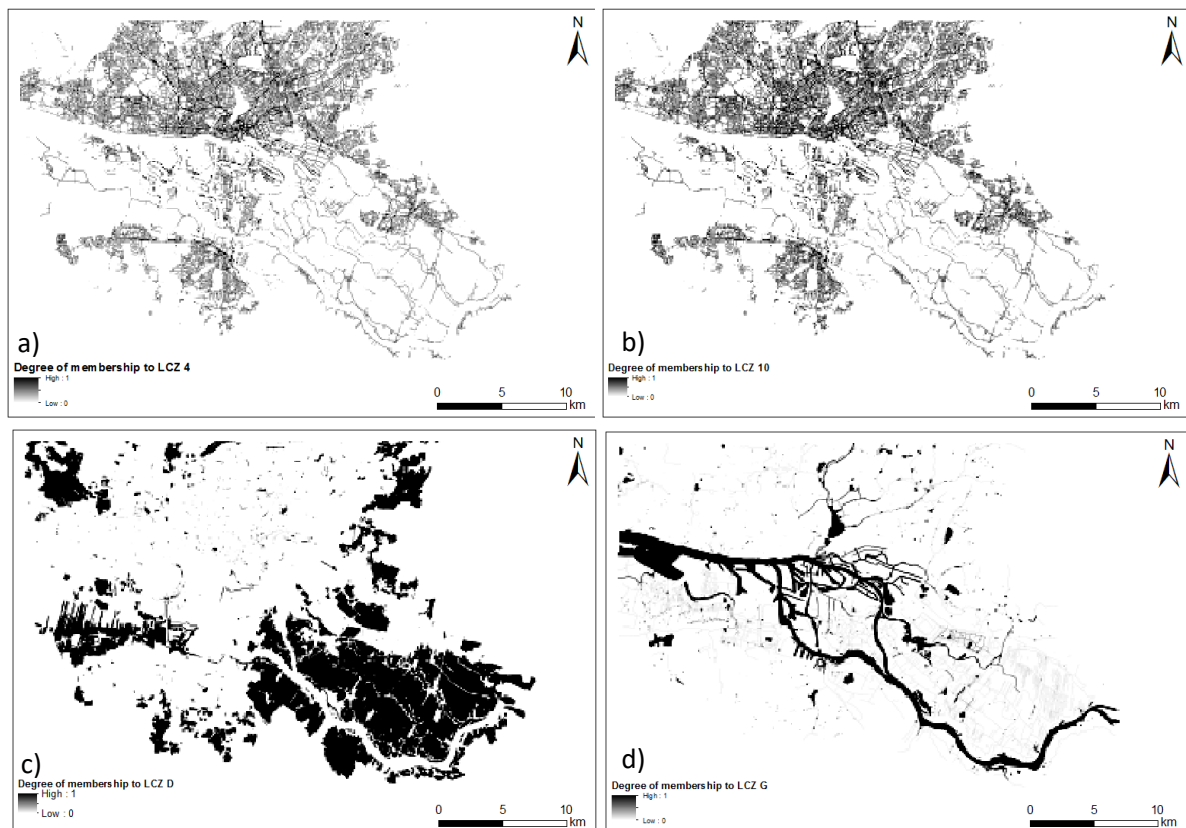


Figure 12 – Degrees of membership of each pixel to the classes a) LCZ 4 (Open high-rise), b) LCZ 10 (Heavy industry), c) LCZ D (Low plants) and d) LCZ G (Water) obtained by converting OSM data to LCZ classes.

The data extracted from OSM will be associated to some pixels with more than one possible LCZ class because there may be overlapping data in OSM that will be assigned to different LCZ classes. However, this will occur mainly for the urban LCZ classes because using only the available BSF and ISF does not enable classes to be identified that are differentiated mainly by building height.

The maximum degrees of membership to the LCZ classes may be considered for assigning the candidate classes to each pixel based on OSM data. However, there may still be pixels with more than one candidate class, as the maximum degree of membership computed as described in section 3.3.2 may be obtained for more than one class. Figure 13 shows the number of candidate classes for each pixel considering this approach. It can be seen that in the urban areas, there are mainly two candidate classes, which are classes LCZ 6 and LCZ 10. Figure 14 a) to d) show, respectively, the obtained locations of cells with candidates in classes LCZ 4, 5, 6 and 10. It can be seen that the regions that are candidates to LCZ classes 4 and 5 are also candidates to class LCZ 6. This happens because the ranges indicated in Table 3 for the BSF are the same for the three classes and the range defined for LCZ 6 contains the intervals defined for both LCZ classes 4 and 5. Therefore, the degree of membership to LCZ 6 will always be larger or equal to the degrees of membership obtained for LCZ 4 or 5. Most of these pixels are also assigned to LCZ class 10 because their BSF is between 20% and 30%, and therefore the same maximum degree of membership will be obtained for the four classes. In the regions where only LCZ 6 and 10 classes are obtained, the value of the ISF is lower. Therefore, as the lower boundary of the ISF interval corresponding to LCZ classes 6 and 10 is 10% lower than the one corresponding to classes LCZ 4 and 5 (see Table 3), the degree of membership to these last classes will also be lower and they are therefore not considered as candidates.

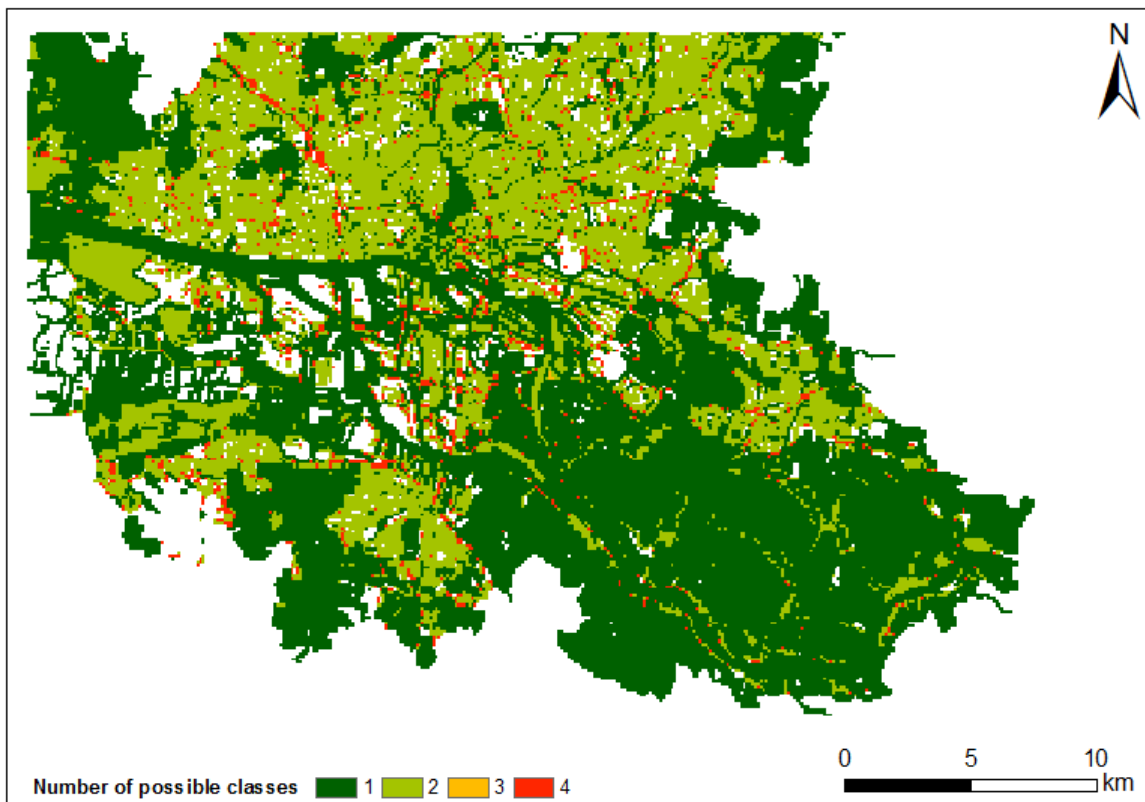


Figure 13 – Number of candidate LCZ classes that can be associated to each pixel considering the maximum degree of membership to each class obtained by converting OSM data to LCZ classes.

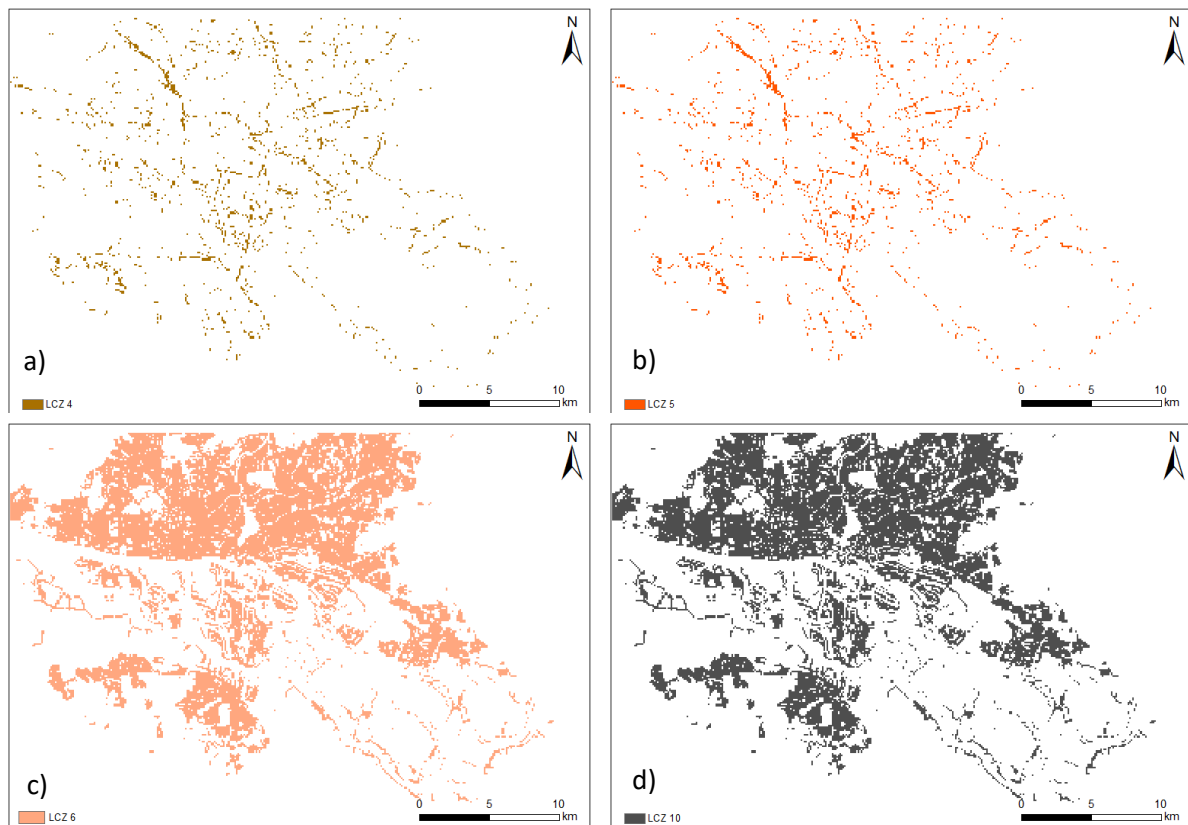


Figure 14 – Pixels that have candidate LCZ classes a) LCZ 4, b) LCZ 5, c) LCZ 6 and d) LCZ 10 considering the maximum degree of membership to each class obtained by converting OSM data to LCZ classes.

4.3 Combination of the results

To assess the influence of OSM data when combining the data using the approach described in section 3.4, several tests were made considering different weights per class and per data source. Table 6 shows the weights assigned to each class for each data source for five different tests undertaken as described below.

In Test 1, the same weight was assigned to the classifications of the four images for all classes, and zero weights were applied to the OSM data. The aim of this test is to compare the results with and without the use of OSM data. In Test 2, the same weights were assigned to all data sources (the classification of the images and OSM-derived data) for all classes. Test 3 considers only the classification of the winter image (the one with best classification results) and OSM, assigning equal weights to both data sources for all classes, except class LCZ G (Water), for which a weight of 60% was assigned to OSM data and 40% to the classification results, because the water class is usually well represented in OSM. Test 4 is similar to test 3, but instead of the winter image, it considers the autumn image (the one with the poorest classification results). Finally, Test 5 considers equal weights for all data sources for the urban LCZ classes, except for LCZ 10, where a higher weight is assigned to the winter image. This is because it can be easily seen by visual analysis that the other classified images have many regions incorrectly classified as LCZ 10, and OSM data are not very reliable for the urban LCZ classes because it does not contain important information needed to identify them uniquely. For the natural classes, equal weights were assigned to all data sources for classes LCZ A and B, while for class LCZ D, a higher weight was assigned to the classification of the winter image, as it can be easily seen by a visual inspection that several regions that should have

been classified as class LCZ D in the other images were wrongly classified as belonging to other classes. The same was done for class LCZ G, but in this case a larger weight was assigned to the data coming from OSM.

Table 6 – Weights assigned to each class and each data source in the tests made to assess the influence of OSM data in the accuracy of the final map.

Test 1											
Classes \ Data	LCZ 1	LCZ 2	LCZ 4	LCZ 5	LCZ 6	LCZ 8	LCZ10	LCZ A	LCZ B	LCZ D	LCZ G
Winter image	20	20	20	20	20	20	20	20	20	20	20
Autumn image	20	20	20	20	20	20	20	20	20	20	20
Summer image	20	20	20	20	20	20	20	20	20	20	20
Spring image	20	20	20	20	20	20	20	20	20	20	20
OSM data	0	0	0	0	0	0	0	0	0	0	0
Test 2											
Classes \ Data	LCZ 1	LCZ 2	LCZ 4	LCZ 5	LCZ 6	LCZ 8	LCZ10	LCZ A	LCZ B	LCZ D	LCZ G
Winter image	20	20	20	20	20	20	20	20	20	20	20
Autumn image	20	20	20	20	20	20	20	20	20	20	20
Summer image	20	20	20	20	20	20	20	20	20	20	20
Spring image	20	20	20	20	20	20	20	20	20	20	20
OSM data	20	20	20	20	20	20	20	20	20	20	20
Test 3											
Classes \ Data	LCZ 1	LCZ 2	LCZ 4	LCZ 5	LCZ 6	LCZ 8	LCZ10	LCZ A	LCZ B	LCZ D	LCZ G
Winter image	50	50	50	50	50	50	50	50	50	50	40
Autumn image	0	0	0	0	0	0	0	0	0	0	0
Summer image	0	0	0	0	0	0	0	0	0	0	0
Spring image	0	0	0	0	0	0	0	0	0	0	0
OSM data	50	50	50	50	50	50	50	50	50	50	60
Test 4											
Classes \ Data	LCZ 1	LCZ 2	LCZ 4	LCZ 5	LCZ 6	LCZ 8	LCZ10	LCZ A	LCZ B	LCZ D	LCZ G
Winter image	0	0	0	0	0	0	0	0	0	0	0
Autumn image	50	50	50	50	50	50	50	50	50	50	40
Summer image	0	0	0	0	0	0	0	0	0	0	0
Spring image	0	0	0	0	0	0	0	0	0	0	0
OSM data	50	50	50	50	50	50	50	50	50	50	60
Test 5											
Classes \ Data	LCZ 1	LCZ 2	LCZ 4	LCZ 5	LCZ 6	LCZ 8	LCZ10	LCZ A	LCZ B	LCZ D	LCZ G
Winter image	20	20	20	20	20	20	40	20	20	40	15
Autumn image	20	20	20	20	20	20	15	20	20	15	15
Summer image	20	20	20	20	20	20	15	20	20	15	15
Spring image	20	20	20	20	20	20	15	20	20	15	15
OSM data	20	20	20	20	20	20	15	20	20	15	40

Figure 15 a) to e) shows the results of the data combination, respectively, for Tests 1 to 5. Differences can be seen mainly for LCZ 10 (Heavy industry), LCZ D (Low plants) and LCZ G (Water). Detailed results of regions with water are obtained when larger weights for this class are assigned to the data extracted from OSM and only one additional data source is considered (Tests 3 and 4, Figure 15 c and d). When additional data are considered, even if a larger weight is assigned to the water data extracted from OSM, its influence in the final result will be less, because the other sources of data did not classify most of the water regions as water, and therefore there is more evidence contradicting the assignment of water to many of these pixels.

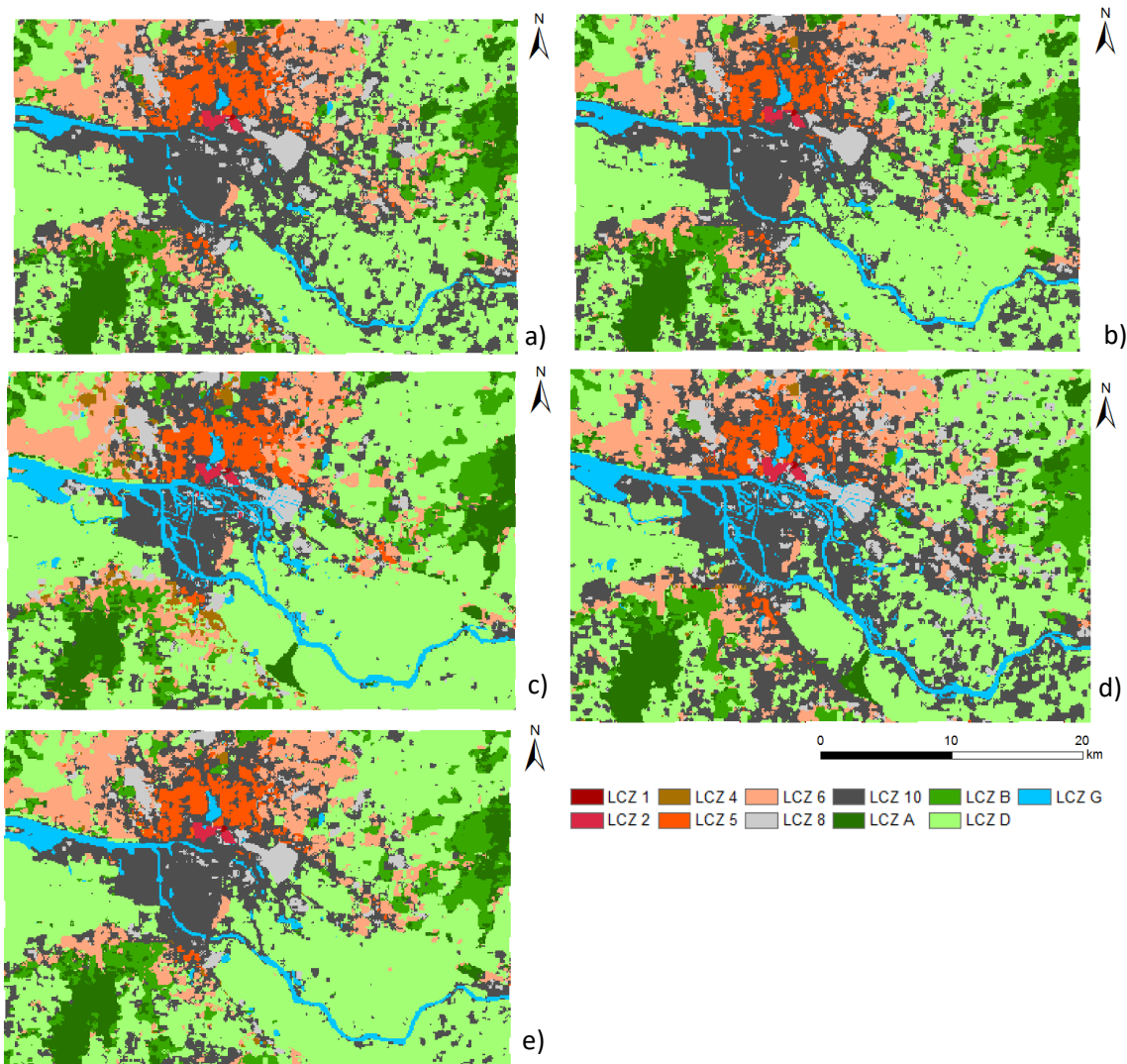


Figure 15 – Combination results using the weights indicated in Table 6 where the figures correspond to a) Test 1, b) Test 2, c) Test 3, d) Test 4 and e) Test 5.

The differences observed for class LCZ 10 and LCZ D show that using OSM data resulted in the correct classification of agricultural regions as LCZ D, which were previously classified incorrectly as LCZ 10 (Tests 1 and 2, Figure 15a and b).

Table 7 shows the accuracy of the results of Tests 1 to 5, obtained with the same reference data used to assess the accuracy of the classified images (see Table 5).

When comparing the results obtained with Tests 1 and 2 (combination of data with and without OSM data), it can be seen that OSM enabled an increase in the overall accuracy from 63% to 68% and the user's and producer's accuracy improved for all the natural classes, except for the producer's accuracy of LCZ G (Water), which decreased from 100% to 90%. However, the user's and producer's accuracy decreased slightly or was kept unchanged for most urban classes, except for LCZ 6 and 10, where both increased slightly in accuracy. This demonstrates that the OSM data were mainly useful in improving the classification of natural areas. Even though the classification of the autumn, summer and spring images had overall accuracies ranging between 53% and 58%, i.e. much lower than the overall accuracy of the classification of the winter image (69%), the combination of all results using OSM data resulted in an overall accuracy very close to that of the best classified image (68%).

Table 7 – User's Accuracy (UA), Producer's Accuracy (PA) and overall accuracy of the results of the combinations corresponding to tests 1 to 5.

LCZ class	Test 1		Test 2		Test 3		Test 4		Test 5	
	UA	PA	UA	PA	UA	PA	UA	PA	UA	PA
LCZ 1	80	41	80	40	79	43	84	44	80	37
LCZ 2	75	63	65	61	76	9	73	52	75	57
LCZ 4	12	6	6	3	82	28	5	6	7	4
LCZ 5	64	69	55	66	77	67	51	56	61	71
LCZ 6	51	71	53	75	45	60	45	65	49	73
LCZ 8	71	25	63	25	79	43	61	32	71	30
LCZ 10	72	54	78	56	59	56	68	53	75	56
LCZ A	65	63	66	63	69	63	47	50	61	61
LCZ B	36	35	38	35	51	46	48	51	53	43
LCZ D	63	93	71	94	75	95	60	91	78	94
LCZ G	60	100	71	90	88	65	84	56	75	84
Overall accuracy	63		68		68		60		70	

Tests 3 and 4 showed that for the classification of the winter image, OSM data had little influence over the accuracy indices, even though it can be seen that due to the slightly larger weight given to water in OSM, the water regions are mapped in much more detail (e.g. compare Figure 9a with Figure 15c). A similar result can be observed for Test 4 made with the classification of the autumn image; however in this case, the overall accuracy increased from 53% to 60%.

Test 5, where the weights were assigned based on which data source provided better results for the different classes, showed an improvement in the overall accuracy, which reached 70%, even though LCZ 4 was still very poorly classified. However, as this class (Open high-rise) is only present in very small areas, it had less influence on the overall accuracy.

4.4 Discussion

The improvements by incorporating OSM data and the fuzzy approach were relatively minor (5% increase between Test 1 and Test 2, 1-17% higher OA of Test 5 compared to seasonal LCZ classifications), yet they are in the same order of magnitude of improvements that others have achieved by incorporating different data and methods. For instance, Xu et al. (2017) reported increases in OA of 3-4%, Tuia et al. (2017) increases of about 2 % in OA but almost 5% in average accuracy, and Verdonck et al. (2017) increases in OA of 5-13% for different cities compared to the WUDAPT standard approach. However, these results are very difficult to compare, since different reference data and validation strategies were applied (cross-validation or separate set, sampling on polygons, pixels, or cities), which are not directly comparable (Bechtel et al., 2019). Moreover, the OA does not indicate the climatic impact, which may be much higher when confusion occurs between fundamentally different classes, as was the case here between heavy industry (LCZ 10) and low plants (LCZ D). Therefore, the standard WUDAPT accuracy assessment also uses a weighted accuracy to account for the climatic differences (Bechtel et al. 2019).

Despite the small increase in OA by incorporating OSM data in this study, the method yields a number of general advantages. First, it easily allows for the incorporation of data of different quality and from different sources, which is not limited to OSM. Secondly, the fuzzy approach could also take advantage of the probabilities derived from the Random Forest classifier and could, thus, be used for probabilistic post-processing. This could also include spatial information and replace the current majority filtering in the WUDAPT protocol. Moreover, it

allows a manual assessment of the relevance of different input data sets, since different weights and combinations can quickly be computed and compared. For this study different multi-seasonal maps were used as inputs in addition to OSM. This confirmed the relevance of multi-temporal data in the WUDAPT approach (Bechtel and Daneke, 2012; Demuzere et al., 2019), since certain classes can be discriminated better in particular seasons due to plant phenology and crop status. Despite the clear added value of the OSM data, this study also confirmed the high relevance of multi-spectral and multi-seasonal data that is already used in LCZ mapping.

5. Conclusions

The WUDAPT project has adopted the LCZ classification scheme as a way of characterizing all cities globally. It recommends a methodology to create the LCZ maps using freely available satellite imagery and software. To date, LCZ maps have been developed for many cities around the world but the quality assurance of these maps indicates that there could still be further improvements in both the methodology and in the data used to create the maps. Moreover, it has been shown that both the choice of the image, i.e., which season, and human influence can have a large impact on the quality of the resulting maps. To address this issue, this paper examined the benefits of using data from OSM to enhance the resulting LCZ map representation and accuracy. A method was developed to convert OSM data to LCZ classes and combine the LCZ maps created through the WUDAPT methodology with the OSM derived LCZ classes using a fuzzy logic approach and a weighted combination method. We demonstrated that different weights can be assigned to the outputs of the classification from different seasonal satellite images as well as the OSM data, based on both those classes and images that may provide more reliable results for a given LCZ class. The confidence that can be associated with the data available in OSM was also calculated. We showed that there are accuracy gains to be had in improving certain classes, e.g., the misclassification of agricultural areas as heavy industry, but there were clear limitations in differentiating between classes that were separated by building heights, in particular LCZ 4. Although there is a tag associated with building height in OSM, this value is rarely filled in by the volunteers. However, with projects such as “OSM Buildings” (Marsch, 2018), which provides 3D views of buildings, the volunteers may become more interested in assigning the number of floors to the buildings, so that realistic and attractive 3D views become available. These data would be enough to extract additional valuable data for differentiating between LCZ urban classes. New sources of free building height data are also becoming available, e.g. through the Urban Atlas for capital cities, which may help to further differentiate between these urban classes in combination with OSM data in the future.

The same reference data were used to assess the accuracy of all the results. Even though there were no major changes in the study area between the first and last date of the images used (2014 and 2017), this may, however, be a cause of small errors in the accuracy results although we consider these as minor.

In this paper, OSM data were only used to identify a class after the LCZ maps were created from the satellite images. However, a clear avenue for future research is to use the data extracted from OSM directly in the training process, e.g. using some regions for training areas and/or merging satellite image classification with OSM extracted data before the recommended spatial filtering is applied. The approach developed here relies on good spatial coverage of data within OSM, which is not always the case for all cities around the world.

However, use of OSM for additional training data would not require the spatial coverage to be as comprehensive.

Finally, the conversion from OSM data to LCZ classes needs to be automated and made available, e.g., as a service in the WUDAPT portal, so that the conversion can be made more easily and the data can be used to assist in the creation of LCZ maps for other cities of the world. Additional processing steps may also be incorporated in a tool designed to implement this service, such as eliminating inconsistencies in OSM data prior to the conversion to LCZ classes (Fonte et al., 2017b; Samsonov and Trigub, 2017) or using additional OSM features to compute buffers around linear features.

Acknowledgements

The study has been partly supported by the Portuguese Foundation for Science and Technology (FCT) under project grant UID/MULTI/ 00308/2013 (CF).

References

- Alexander, P.J., Bechtel, B., Chow, W.T.L., Fealy, R., Mills, G., 2016. Linking urban climate classification with an urban energy and water budget model: Multi-site and multi-seasonal evaluation. *Urban Clim.* 17, 196–215. <https://doi.org/10.1016/j.uclim.2016.08.003>
- Bechtel, B., Alexander, P.J., Beck, C., Böhner, J., Brousse, O., Ching, J., Demuzere, M., Fonte, C., Gál, T., Hidalgo, J., Hoffmann, P., Middel, A., Mills, G., Ren, C., See, L., Sismanidis, P., Verdonck, M.-L., Xu, G., Xu, Y., 2019. Generating WUDAPT Level 0 data – Current status of production and evaluation. *Urban Clim.* 27, 24–45. <https://doi.org/10.1016/j.uclim.2018.10.001>
- Bechtel, B., Alexander, P.J., Böhner, J., Ching, J., Conrad, O., Feddema, J., Mills, G., See, L., Stewart, I., 2015. Mapping Local Climate Zones for a worldwide database of the form and function of cities. *ISPRS Int. J. Geo-Inf.* 4, 199–219. <https://doi.org/10.3390/ijgi4010199>
- Bechtel, B., Daneke, C., 2012. Classification of Local Climate Zones based on multiple Earth Observation data. *IEEE J. Sel. Top. Appl. Earth Obs. Remote Sens.* 5, 1191–1202. <https://doi.org/10.1109/JSTARS.2012.2189873>
- Bechtel, B., Demuzere, M., Mills, G., Zhan, W., Sismanidis, P., Small, C., Voogt, J.A., in review. SUHI analysis using Local Climate Zones. *Urban Clim.*
- Bechtel, B., Demuzere, M., Sismanidis, P., Fenner, D., Brousse, O., Beck, C., Van Coillie, F., Conrad, O., Keramitsoglou, I., Middel, A., Mills, G., Niyogi, D., Otto, M., See, L., Verdonck, M.-L., 2017. Quality of Crowdsourced Data on Urban Morphology—The Human Influence Experiment (HUMINEX). *Urban Sci.* 1, 15. <https://doi.org/10.3390/urbansci1020015>
- Bechtel, B., See, L., Mills, G., Foley, M., 2016. Classification of Local Climate Zones Using SAR and Multispectral Data in an Arid Environment. *IEEE J. Sel. Top. Appl. Earth Obs. Remote Sens.* 9, 3097–3105. <https://doi.org/10.1109/JSTARS.2016.2531420>
- Bechtel, B., Zakšek, K., Hoshyaripour, G., 2012. Downscaling land surface temperature in an urban area: A case study for Hamburg, Germany. *Remote Sens.* 4, 3184–3200.
- Brousse, O., Martilli, A., Foley, M., Mills, G., Bechtel, B., 2016. WUDAPT, an efficient land use producing data tool for mesoscale models? Integration of urban LCZ in WRF over Madrid. *Urban Clim.* 17, 116–134. <https://doi.org/10.1016/j.uclim.2016.04.001>
- Card, D.H., 1982. Using known map category marginal frequencies to improve estimates of thematic map accuracy. *Photogramm. Eng. Remote Sens.* 48, 431–439.
- Ching, J., Mills, G., Bechtel, B., See, L., Feddema, J., Wang, X., Ren, C., Brousse, O., Martilli, A., Neophytou, M., Mouzourides, P., Stewart, I., Hanna, A., Ng, E., Foley, M., Alexander, P., Aliaga, D., Niyogi, D., Shreevastava, A., Bhalachandran, P., Masson,

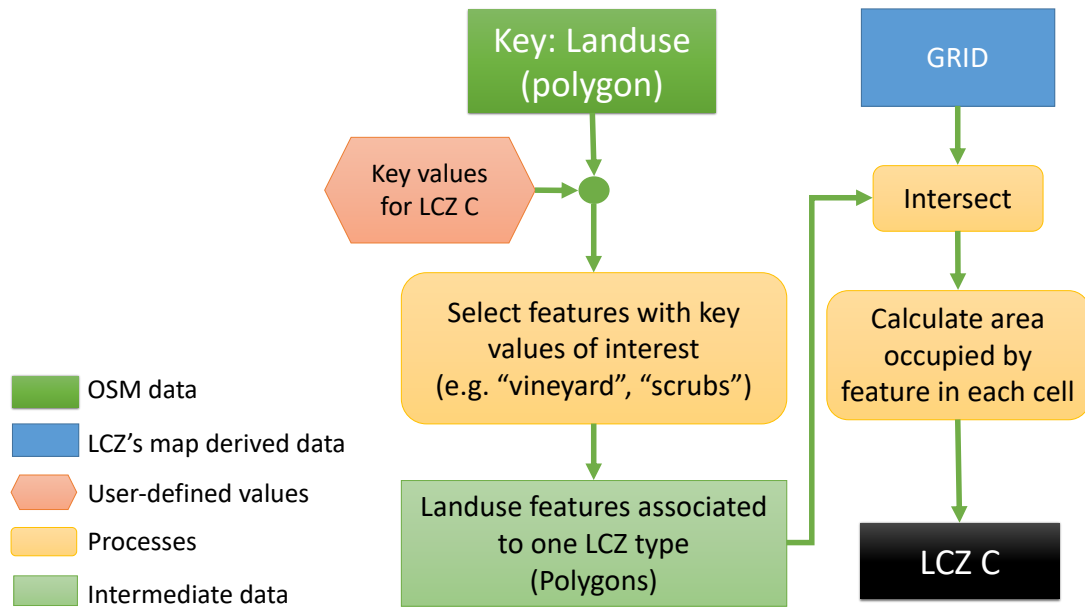
- V., Hidalgo, J., Fung, J., Andrade, M., Baklanov, A., Dai, W., Milcinski, G., Demuzere, M., Brunzell, N., Pesaresi, M., Miao, S., Mu, Q., Chen, F., Theeuwes, N., 2018. World Urban Database and Access Portal Tools (WUDAPT), an urban weather, climate and environmental modeling infrastructure for the Anthropocene. *Bull. Am. Meteorol. Soc.* <https://doi.org/10.1175/BAMS-D-16-0236.1>
- Coast, S., 2005. OpenStreetMap. *Bull. Soc. Cartogr.* 39, 62.
- Demuzere, M., Bechtel, B., Middel, A., Mills, G., in review. Mapping Europe into Local Climate Zones. *PLoS ONE*.
- Demuzere, M., Bechtel, B., Mills, G., 2019. Global transferability of local climate zone models. *Urban Clim.* 27, 46–63. <https://doi.org/10.1016/j.uclim.2018.11.001>
- Fan, H., Zipf, A., Fu, Q., Neis, P., 2014. Quality assessment for building footprints data on OpenStreetMap. *Int. J. Geogr. Inf. Sci.* 28, 700–719. <https://doi.org/10.1080/13658816.2013.867495>
- Fonte, C., Minghini, M., Patriarca, J., Antoniou, V., See, L., Skopeliti, A., 2017a. Generating up-to-date and detailed land use and land cover maps using OpenStreetMap and GlobeLand30. *ISPRS Int. J. Geo-Inf.* 6, 125. <https://doi.org/10.3390/ijgi6040125>
- Fonte, C., Patriarca, J., Minghini, M., Antoniou, V., See, L., Brovelli, M., 2017b. Using OpenStreetMap to Create Land Use and Land Cover Maps: Development of an Application, in: Calazans Campelo, C.E., Bertolotto, M., Corcoran, P. (Eds.), *Volunteered Geographic Information and the Future of Geospatial Data, Advances in Geospatial Technologies*. IGI Global, Hershey, PA, USA. <https://doi.org/10.4018/978-1-5225-2446-5>
- Gal, T., Bechtel, B., Lelovics, E., 2015. Comparison of two different Local Climate Zone mapping methods, in: *Proceedings of the ICUC9*. Presented at the ICUC9, Meteo France, Toulouse, France.
- Geletič, J., Lehnert, M., 2016. GIS-based delineation of local climate zones: The case of medium-sized Central European cities. *Morav. Geogr. Rep.* 24, 2–12. <https://doi.org/10.1515/mgr-2016-0012>
- Girres, J.-F., Touya, G., 2010. Quality assessment of the French OpenStreetMap dataset. *Trans. GIS* 14, 435–459.
- Goodchild, M.F., 2007. Citizens as sensors: The world of volunteered geography. *GeoJournal* 69, 211–221.
- Grippa, T., Georganos, S., Zarougui, S., Bognounou, P., Diboulo, E., Forget, Y., Lennert, M., Vanhuysse, S., Mboga, N., Wolff, E., 2018. Mapping urban land use at street block level using OpenStreetMap, remote sensing data, and spatial metrics. *ISPRS Int. J. Geo-Inf.* 7, 246. <https://doi.org/10.3390/ijgi7070246>
- Gugler, J., 1996. *The Urban Transformation of the Developing World*. Oxford University Press, New York.
- Haklay, M. (Muki), Basiouka, S., Antoniou, V., Ather, A., 2010. How Many Volunteers Does it Take to Map an Area Well? The Validity of Linus' Law to Volunteered Geographic Information. *Cartogr. J.* 47, 315–322. <https://doi.org/10.1179/000870410X12911304958827>
- Haklay, M., Weber, P., 2008. OpenStreet map: User-generated street maps. *IEEE Pervasive Comput.* 7, 12–18.
- Hammerberg, K., Brousse, O., Martilli, A., Mahdavi, A., 2018. Implications of employing detailed urban canopy parameters for mesoscale climate modelling: a comparison between WUDAPT and GIS databases over Vienna, Austria. *Int. J. Climatol.* 38, e1241–e1257. <https://doi.org/10.1002/joc.5447>
- Harlan, S.L., Ruddell, D.M., 2011. Climate change and health in cities: impacts of heat and air pollution and potential co-benefits from mitigation and adaptation. *Curr. Opin. Environ. Sustain.* 3, 126–134. <https://doi.org/10.1016/j.cosust.2011.01.001>
- Hidalgo, J., Dumas, G., Masson, V., Gwendall, P., Bechtel, B., Bocher, E., Foley, M., Schoetter, R., Mills, G., accepted. Comparison between Local Climate Zones maps derived from administrative datasets and satellite observations. *Urban Clim.*

- Jokar Arsanjani, J., Zipf, A., Mooney, P., Helbich, M. (Eds.), 2015. *OpenStreetMap in GIScience, Lecture Notes in Geoinformation and Cartography*. Springer International Publishing, Cham, Switzerland.
- Kaloustian, N., Tammimga, M., Bechtel, B., 2017. Local climate zones and annual surface thermal response in a Mediterranean city, in: *Urban Remote Sensing Event (JURSE), 2017 Joint. IEEE*, pp. 1–4.
- Klir, G.J., Yuan, B., 1995. *Fuzzy Sets and Fuzzy Logic: Theory and Applications*, 1st edition. ed. Prentice Hall, Upper Saddle River, N.J.
- Lelovics, E., Unger, J., Gál, T., Gál, C., 2014. Design of an urban monitoring network based on Local Climate Zone mapping and temperature pattern modelling. *Clim. Res.* 60, 51–62. <https://doi.org/10.3354/cr01220>
- Lopes, P., Fonte, C., See, L., Bechtel, B., 2017. Using OpenStreetMap data to assist in the creation of LCZ maps, in: *2017 Joint Urban Remote Sensing Event (JURSE). Presented at the 2017 Joint Urban Remote Sensing Event (JURSE), IEEE, Dubai, United Arab Emirates*, pp. 1–4. <https://doi.org/10.1109/JURSE.2017.7924630>
- Marsch, J., 2018. OSM Buildings. Available at: <https://osmbuildings.org/>.
- Mitraka, Z., Del Frate, F., Chrysoulakis, N., Gastellu-Etchegorry, J.-P., 2015. Exploiting Earth Observation data products for mapping Local Climate Zones, in: *Urban Remote Sensing Event (JURSE), 2015 Joint. IEEE*, pp. 1–4.
- Mooney, P., 2015. Quality assessment of the contributed land use information from OpenStreetMap versus authoritative datasets, in: *Jokar Arsanjani, J., Zipf, A., Mooney, P., Helbich, M. (Eds.), OpenStreetMap in GIScience, Lecture Notes in Geoinformation and Cartography*. Springer International Publishing, Cham, pp. 319–324.
- Neis, P., Zielstra, D., 2014. Recent developments and future trends in volunteered geographic information research: The case of OpenStreetMap. *Future Internet* 6, 76–106. <https://doi.org/10.3390/fi6010076>
- Ngie, A., Abutaleb, K., Ahmed, F., Darwish, A., Ahmed, M., 2014. Assessment of urban heat island using satellite remotely sensed imagery: a review. *South Afr. Geogr. J.* 96, 198–214. <https://doi.org/10.1080/03736245.2014.924864>
- Oke, T., 1967. City size and the Urban Heat Island. *Atmos. Environ.* 7, 769–779.
- Oke, T.R., 1982. The energetic basis of the urban heat island. *Quarterly J R. Meteorol Soc* 108, 1–24.
- Oke, T.R., Mills, G., Christen, A., Voogt, J.A., 2017. *Urban Climates*. Cambridge University Press.
- OpenStreetMap Wiki contributors, 2018. Map Features. Available online at: http://wiki.openstreetmap.org/w/index.php?title=Map_Features&oldid=1687489.
- Qiu, C., Schmitt, M., Mou, L., Ghamisi, P., Zhu, X., Qiu, C., Schmitt, M., Mou, L., Ghamisi, P., Zhu, X.X., 2018. Feature Importance Analysis for Local Climate Zone Classification Using a Residual Convolutional Neural Network with Multi-Source Datasets. *Remote Sens.* 10, 1572. <https://doi.org/10.3390/rs10101572>
- Revi, A., Satterthwaite, D., Aragon-Durand, F., et al., 2014. Urban areas. In: *Climate Change 2014: Impacts, Adaptation, and Vulnerability. Part A: Global and Sectoral Aspects. Contribution of Working Group II to the Fifth Assessment Report of the Intergovernmental Panel on Climate Change [Field, C.B., V.R. Barros, D.J. et al. (eds.)]*. Cambridge University Press, Cambridge, United Kingdom and New York, NY, USA, pp. 535-612.
- Rose, J., Wilke, C.B., 2015. *Climate Change Vulnerability in Cities – the Case of Hamburg*. Hamburg Institute of International Economics (HWWI), Hamburg. Available online at: http://www.hwwi.org/fileadmin/hwwi/Publikationen/Research/HWWI_ResearchPaper_167-kl.pdf.
- Samsonov, T., Trigub, K., 2017. Towards computation of urban local climate zones (LCZ) from Openstreetmap data, in: *Proceedings of the 14th International Conference on GeoComputation. Presented at the 14th International Conference on GeoComputation, Leeds, UK*, pp. 1–9.

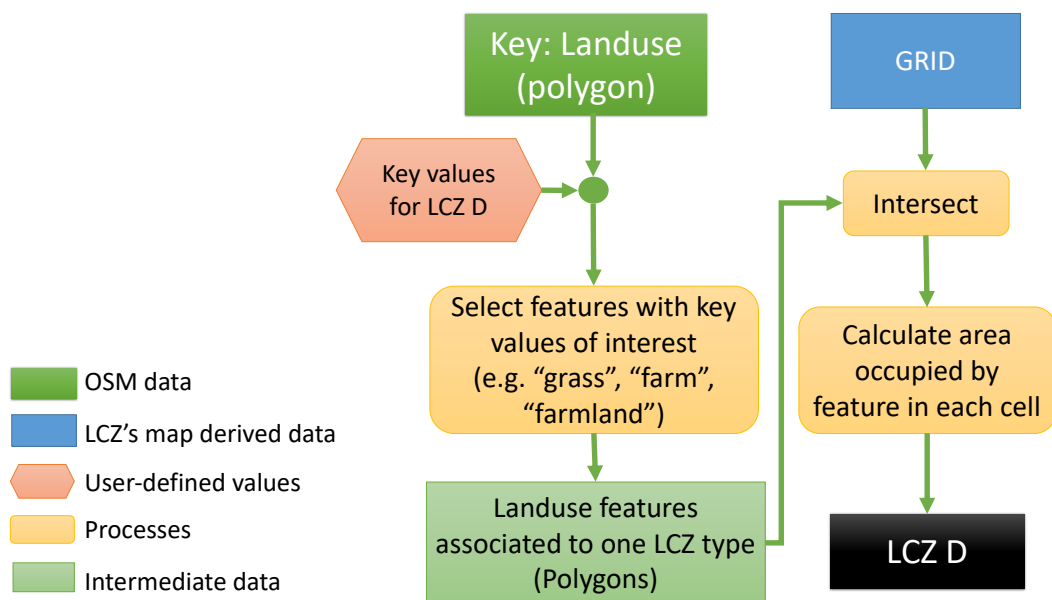
- Santamouris, M., 2014. Analysing the heat island magnitude and characteristics in one hundred Asian and Australian cities and regions. Landscape and Urban Planning Working Paper.
- Schultz, M., Voss, J., Auer, M., Carter, S., Zipf, A., 2017. Open land cover from OpenStreetMap and remote sensing. *Int. J. Appl. Earth Obs. Geoinformation* 63, 206–213. <https://doi.org/10.1016/j.jag.2017.07.014>
- Statistical Office of Hamburg and Schleswig-Holstein, 2014. Facts and Figures. Grafik & Druck GmbH & Co KG, Kiel. Available online at: https://www.statistiknord.de/fileadmin/Dokumente/Faltblätter/Faltblatt_Stadtportrait_2013_E_Internet.pdf.
- Stewart, I.D., Oke, T.R., 2012. Local Climate Zones for Urban Temperature Studies. *Bull. Am. Meteorol. Soc.* 93, 1879–1900. <https://doi.org/10.1175/BAMS-D-11-00019.1>
- Stewart, I.D., Oke, T.R., Krayenhoff, E.S., 2014. Evaluation of the 'local climate zone' scheme using temperature observations and model simulations. *Int. J. Climatol.* 34, 1062–1080. <https://doi.org/10.1002/joc.3746>
- Sukhanov, S., Tankoyeu, I., Louradour, J., Heremans, R., Trofimova, D., Debes, C., 2017. Multilevel ensembling for local climate zones classification, in: 2017 IEEE International Geoscience and Remote Sensing Symposium (IGARSS). Presented at the 2017 IEEE International Geoscience and Remote Sensing Symposium (IGARSS), pp. 1201–1204. <https://doi.org/10.1109/IGARSS.2017.8127173>
- Tomlinson, C.J., Chapman, L., Thornes, J.E., Baker, C., 2011. Remote sensing land surface temperature for meteorology and climatology: a review: Remote sensing land surface temperature. *Meteorol. Appl.* 18, 296–306. <https://doi.org/10.1002/met.287>
- Tuia, D., Moser, G., Saux, B.L., Bechtel, B., See, L., 2017a. 2017 IEEE GRSS Data Fusion Contest: Open Data for Global Multimodal Land Use Classification [Technical Committees]. *IEEE Geosci. Remote Sens. Mag.* 5, 70–73. <https://doi.org/10.1109/MGRS.2016.2645380>
- Tuia, D., Moser, G., Wurm, M., Taubenböck, H., 2017b. Land use modeling in North Rhine-Westphalia with interaction and scaling laws, in: 2017 Joint Urban Remote Sensing Event (JURSE). Presented at the 2017 Joint Urban Remote Sensing Event (JURSE), pp. 1–4. <https://doi.org/10.1109/JURSE.2017.7924542>
- Tzavali, A., Paravantis, J.P., Mihalakakou, G., Fotiadi, A., Stigka, E., 2015. Urban heat island intensity: A literature review. *Fresenius Environ. Bull.* 24, 4537–4551.
- UN Department of Economic and Social Affairs, 2017. World Population Prospects. Available online at: <https://www.un.org/development/desa/publications/world-population-prospects-the-2017-revision.html>.
- UNEP, 2004. Impacts of summer 2003 heat wave in Europe; Environment Alert Bulletin.
- Unger, J., Lelovics, E., Gál, T., 2014. Local Climate Zone mapping using GIS methods in Szeged. *Hung. Geogr. Bull.* 63, 29–41.
- Verdonck, M.-L., Okujeni, A., van der Linden, S., Demuzere, M., De Wulf, R., Van Coillie, F., 2017. Influence of neighbourhood information on 'Local Climate Zone' mapping in heterogeneous cities. *Int. J. Appl. Earth Obs. Geoinformation* 62, 102–113.
- Wouters, H., Demuzere, M., Blahak, U., Fortuniak, K., Maiheu, B., Camps, J., Tielemans, D., van Lipzig, N.P.M., 2016. The efficient urban canopy dependency parametrization (SURY) v1.0 for atmospheric modelling: description and application with the COSMO-CLM model for a Belgian summer. *Geosci Model Dev* 9, 3027–3054. <https://doi.org/10.5194/gmd-9-3027-2016>
- Xu, Y., Ma, F., Meng, D., Ren, C., Leung, Y., 2017. A co-training approach to the classification of local climate zones with multi-source data, in: 2017 IEEE International Geoscience and Remote Sensing Symposium (IGARSS). Presented at the 2017 IEEE International Geoscience and Remote Sensing Symposium (IGARSS), pp. 1209–1212. <https://doi.org/10.1109/IGARSS.2017.8127175>
- Xu, Yong, Ren, C., Cai, M., Edward, N.Y.Y., Wu, T., 2017. Classification of Local Climate Zones Using ASTER and Landsat Data for High-Density Cities. *IEEE J. Sel. Top. Appl. Earth Obs. Remote Sens.*

- Yokoya, N., Ghamisi, P., Xia, J., Sukhanov, S., Heremans, R., Tankoyeu, I., Bechtel, B., Saux, B.L., Moser, G., Tuia, D., 2018. Open Data for Global Multimodal Land Use Classification: Outcome of the 2017 IEEE GRSS Data Fusion Contest. *IEEE J. Sel. Top. Appl. Earth Obs. Remote Sens.* 11, 1363–1377. <https://doi.org/10.1109/JSTARS.2018.2799698>
- Zheng, Y., Ren, C., Xu, Y., Wang, R., Ho, J., Lau, K., Ng, E., 2018. GIS-based mapping of Local Climate Zone in the high-density city of Hong Kong. *Urban Clim.* 24, 419–448. <https://doi.org/10.1016/j.uclim.2017.05.008>

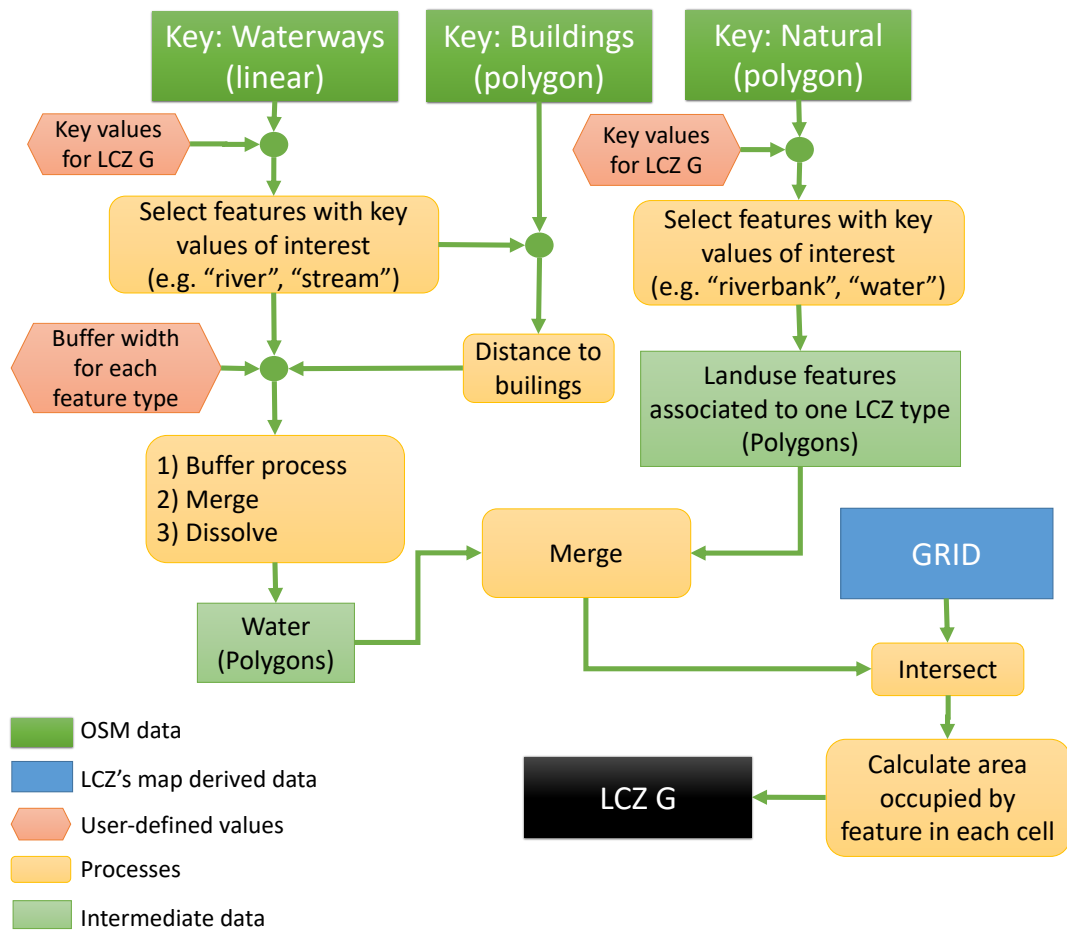
Supplementary materials



Schematic of the methodology used for the conversion of OSM data into LCZ class C (Bush, shrub).



Schematic of the methodology used for the conversion of OSM data into LCZ class D (Low plants).



Schematic of the methodology used for converting OSM to class LCZ G (Water).